# Structural Models of the MscL Gating Mechanism

Sergei Sukharev,* Stewart R. Durell,† and H. Robert Guy†
*Department of Biology, University of Maryland, College Park, Maryland 20742; and †Laboratory of Experimental and Computational Biology, National Cancer Institute, National Institutes of Health, Bethesda, Maryland 20892-5677 USA

ABSTRACT Three-dimensional structural models of the mechanosensitive channel of large conductance, MscL, from the bacteria *Mycobacterium tuberculosis* and *Escherichia coli* were developed for closed, intermediate, and open conformations. The modeling began with the crystal structure of *M. tuberculosis* MscL, a homopentamer with two transmembrane $\alpha$-helices, M1 and M2, per subunit. The first 12 N-terminal residues, not resolved in the crystal structure, were modeled as an amphipathic $\alpha$-helix, called S1. A bundle of five parallel S1 helices are postulated to form a cytoplasmic gate. As membrane tension induces expansion, the tilts of M1 and M2 are postulated to increase as they move away from the axis of the pore. Substantial expansion is postulated to occur before the increased stress in the S1 to M1 linkers pulls the S1 bundle apart. During the opening transition, the S1 helices and C-terminus amphipathic $\alpha$-helices, S3, are postulated to dock parallel to the membrane surface on the perimeter of the complex. The proposed gating mechanism reveals critical spatial relationships between the expandable transmembrane barrel formed by M1 and M2, the gate formed by S1 helices, and "strings" that link S1s to M1s. These models are consistent with numerous experimental results and modeling criteria.

## INTRODUCTION

The mechanosensitive channel of large conductance, MscL, is a ubiquitous component of the bacterial cell envelope providing for fast adjustments of turgor pressure in response to osmotic downshifts. When the membrane tension approaches the lytic limit, MscL forms a large nonselective pore that releases excessive osmolytes, thus acting as a "safety valve." MscL was the first cloned and characterized molecule shown to convert mechanical tension in the membrane into a simple increase in membrane permeability (Sukharev et al., 1994). This apparently purely bacterial protein is of prime biophysical interest because it is a highly convenient molecular system for studies of elemental principles of mechanotransduction. Recent crystallographic determination of the three-dimensional (3D) structure of the MscL homolog from *Mycobacterium tuberculosis* (Chang et al., 1998) has provided a strong framework for precise evaluation of conformations and molecular interactions of the gating mechanism for this relatively simple molecular valve. In addition to the crystal structure, there is a wealth of useful functional information, such as kinetic and thermodynamic parameters for MscL gating (Sukharev et al., 1999), and effects of numerous mutations on tension sensitivity and kinetics (Blount et al., 1996a, 1997; Häse et al., 1997; Liu et al., 1999; Oakley et al., 1999; Ou et al., 1998; Yoshimura et al., 1999).

To better understand the gating mechanism of MscL, we have developed structural models of both TbMscL and EcoMscL in closed, open, and a series of transition conformations. Aspects of the proposed gating mechanism were then tested. We have already presented a brief description of our EcoMscL models and the experimental evidence supporting aspects of them (Sukharev et al., 2001). Here we describe the models, methods, and rationale for developing them in detail. These models are working hypotheses that were generated using subjective computational methods of molecular modeling. This approach necessitates specifying the structure in much more detail than warranted by current experimental data. However, we make no claim that these models are correct at the atomic scale; rather, they are intended only to illustrate general features of the proposed gating mechanism. They assign the protein domains involved in the gating and the directions, angles, and distances for their movements during the transition. Some aspects of the models are less certain than others, in part because some of the experimental constraints are not very precise. We try to warn the reader of these uncertainties and difficulties throughout the text.

The most notable feature of our models is the hypothesis that the N-terminus S1 segment is an integral component of the gating mechanism. The crystal structure of TbMscL (Chang et al., 1998) revealed the general architecture of the pentameric complex for a closed conformation; however, the N-terminus S1 segment was not resolved. The narrowest part of the pore is surrounded by a ring of five valines (V21 in TbMscL or V23 in EcoMscL). These have been postulated to form a gate that prevents ion permeation by posing a hydrophobic barrier. Results of random (Ou et al., 1998) and site-directed (Yoshimura et al., 1999) mutagenesis indicated that hydrophilic substitutions in the narrow region of the pore destabilize the closed state, permitting the channel to open at very low tensions. However, even the most severe "gain-of-function" mutants (such as V23D, in which the hydrophobic barrier is replaced by charged residues), still gate and close completely even though their gating kinetics are altered. This suggests that there is an additional

*Received for publication 25 January 2001 and in final form 9 May 2001.*
Address reprint requests to Dr. H. Robert Guy, NCI, LECB, NIH, Bldg. 12, Room B105, 12 South Drive, Bethesda, MD 20892-5677. Tel.: 301-496-2068; Fax: 301-402-4724; E-mail: bg4y.nih.gov.

0006-3495/01/08/917/20 $2.00

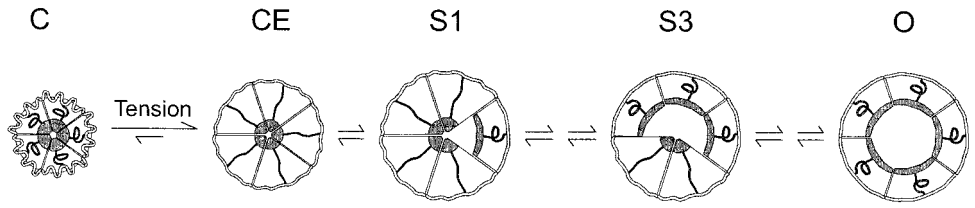


FIGURE 1 Schematic representation of a gating mechanism based on analyses of gating properties (Sukharev et al., 1999). The outer rim is postulated to be the "tension sensor," and can expand substantially before the channel opens. The central "activation gate" is postulated to consistent of five components, which are connected to the tension sensing rim by "strings." The transition from the closed resting conformation, CR, to the closed expanded conformation, CE, is electrically silent and rather elastic. The channel first opens to a subconducting state, S1, when the expansion of the rim places sufficient stress on the strings to cause one of the activation gate components to pull away from the central "gate." The tension dependency of transition from the CE to S1 suggests an in-plane area increase, $\Delta A$, of $\sim$4 nm$^2$. The channel may then pass through more substates, S2 and S3, as the activation gate continues to break down before reaching the fully open conformation, O; however, these latter transitions are relatively tension-independent ($\Delta A \sim$2 nm$^2$ for all), suggesting little expansion of the outer rim.

gate. The tension-independent appearance of subconducting states (Sukharev et al., 1999) described below also suggests that elements other than constriction of the M1 pore strongly interfere with channel conductance.

A two-state kinetic analysis of experimental data from EcoMscL (Sukharev et al., 1999) predicted that the kinetic barrier between the closed and open states occurs when the expansion of the transmembrane in-plane area is about two-thirds that of the open state. In other words, before the channel reaches the top of the barrier and then opens, it must expand considerably. The single-mode closed time distribution usually observed over a wide range of tensions and open probabilities (Chiang, Anishkin, and Sukharev, manuscript in preparation) also suggests that under stretch, the protein experiences continuous and relatively barrier-free elastic deformation before opening.

Time-resolved recordings from EcoMscL revealed at least three transient subconducting states of short duration and a fully open state. A detailed multi-state kinetic analysis predicted the following linear scheme, C$\leftrightarrow$ S1$\leftrightarrow$ S2$\leftrightarrow$ S3$\leftrightarrow$ O, in which the channel passes through the subconducting states as it opens and closes. Only the first transition appeared to be strongly tension-dependent, whereas the others were relatively insensitive. Assuming that the in-plane channel expansion ($\Delta A$) at given membrane tension ($T$) contributes as $T\Delta A$ to the free energy of that particular transition, this result means that the transitions between the latter substates are not associated with any substantial area change. The schematic model of MscL gating illustrated in Fig. 1 was developed to explain these findings. In this model, the rim, or the outer wall of the transmembrane region, acts as a "tension sensor," which is linked to an "activation gate" by radial strings. When the membrane is stretched, the tension sensor expands until enough tension is placed on the strings to pull the activation gate apart. In this model, subconductance states are due to a stepwise breakdown or re-association of the activation gate, which is an assembly of components from each of the five subunits.

We have turned to molecular modeling in an attempt to relate the static crystal structure of *M. tuberculosis* MscL (TbMscL) to the dynamic model of *Escherichia coli* MscL (EcoMscL) gating. Starting with the crystal structure of TbMscL and using available experimental data, we first reconstructed 3D models of the putative native closed conformation for both TbMscL and EcoMscL homologs. By using small translational ($\sim$1 Å) and angular displacements for the transmembrane domains, and changing the conformations of connecting loops, we modeled a sequence of expanded closed, partially open, and fully open states, and predict the path for the transitions. The mechanism suggests that the tension sensor is formed by the M1 and M2 transmembrane helices, that the activation gate is formed by an assembly of five putative N-terminal amphipathic helices (one S1 helix per subunit) that are missing in the crystal structure, and that the strings are formed by the segment linking S1 to M1. The latter permits the initial expansion of the complex without opening, and subsequent pore opening via a number of intermediate conformations that are accompanied by relatively small changes of the in-plane area. These features reflect tension-dependencies for rate constants of conformational changes between the substates observed in experiment, whereas the size of the open pore correlates with the channel conductance. Effects of particular mutations on the channel gating are discussed in the framework of this model. Although the models are hypothetical, they should provide a good starting point for more precise mutagenesis experiments, which in turn should help correct and refine the model.

## METHODS

The general criteria and principles used in developing 3D models of the MscL proteins were as follows (see Durell and Guy, 1999; Guy and Durell, 1994, 1996): 1) the protein should form a solid barrier between the lipid alkyl chains and the aqueous pore in all conformations; 2) segments in contact with the lipid alkyl chains should have a regular secondary struc-

ture; 3) the net charge of the residues interacting with the internal lipid headgroups should be positive; 4) almost all hydrogen bond donor and acceptor atoms should form hydrogen bonds with other protein groups, water, or lipid headgroups; 5) although not essential, preference should be given to structures that allow charged residues in the transmembrane region to be near to, or form salt bridges with, oppositely charged residues; 6) some preference is given to models in which adjacent helices pack according to "knobs-into-holes" (Crick, 1953) and/or "ridges-into-grooves" (Chothia et al., 1981) packing theory (Bowie, 1997a); 7) most backbone and side chain conformations should be energetically favorable and occur frequently in proteins of known conformation (Ponder and Richards, 1987); 8) side chains that are completely exposed to the lipid alkyl chains should be hydrophobic and may be poorly conserved if they are exposed in all conformations (Guy, 1988; Komiya et al., 1988); 9) most highly conserved residues (with the exception of residues such as some prolines that strongly affect the secondary structure) should interact with other highly conserved residues, and should be structurally and/or functionally important.

Several of these criteria are based on statistical tendencies and thus are not absolute. In general, some criteria, e.g., 5 and 6, are weaker than others, and we will violate these to improve satisfaction of the more stringent criteria. However, in the MscL models presented here, all of these criteria are well satisfied.

The assumptions specific for developing the models of the MscL proteins were 1) the transmembrane and periplasmic portions of the crystal structure for *M. tuberculosis* MscL (Chang et al., 1998) is correct for the most closed conformation. (The cytoplasmic segments were considered less informative because the first nine residues of the N-terminus were not resolved); 2) the EcoMscL has a similar backbone structure for those segments that can be aligned unambiguously without insertions or deletions with the sequence from *M. tuberculosis*; 3) the relationship between the more tightly packed transmembrane helices of the crystal structure, M1 of one subunit and M2 of the adjacent subunit, remains relatively unchanged throughout the gating process; 4) the open pore has a diameter between 3 and 4 nm (Cruickshank et al., 1997; Sukharev et al., 1999); 5) the protein has a gate that keeps the channel closed even when the transmembrane region has expanded substantially; 6) during the opening, conformational changes through upper subconducting states are not associated with a substantial change of the area of the protein in the plane of the membrane.

Atomic-scale models of the MscL proteins were developed in the following manner. Idealized $\alpha$-helices were generated for those segments of the EcoMscL analogous to the helices of the TbMscL crystal structure. These were matched to those of *M. tuberculosis* using the PSSHOW modeling program. The side chains of the residues were initially set into the conformation that occurs most often for them in $\alpha$-helices in the protein structure database. Side-chain conformations were then adjusted to avoid steric overlap, and in some cases to form energetically favorable interactions such as salt bridges and hydrogen bonds. For models of intermediate and open conformations and for models of the cytoplasmic region of the closed conformation, the putative $\alpha$-helices were positioned manually and connecting segments were constructed manually before the energy of the structure was minimized using the CHARMM computer program (Brooks et al., 1983). This manual manipulation and minimization procedure was repeated for each conformation until the models were deemed to satisfy the criteria described above. Segments linking helices are the most ambiguous portions of the model; however, they tend to be poorly conserved and their precise conformations are not essential for the general models presented here. The water-exposed areas for residues inside the pore were assessed for two classes of models using the GETAREA 1.1 on-line software (www.scsb.utmb.edu/cgi-bin/get a form.tcl). The difference in energies associated with hydration of the new surface was estimated using a standard hydrophobicity scale (Guy, 1985). The cross-sectional area of the protein complex in the plane of the membrane was calculated based on the solvent-accessible surface built with the $r_{probe} = 5$ Å. Space-filled models were sliced with several planes normal to the axis of channel symmetry, and the cross-sectional area of planar projections was computed using a custom routine written in MatLab. The expansion of the protein was assessed as the average of area changes at three levels along the axis, near lipid headgroups on each side of the membrane and at the membrane midplane.

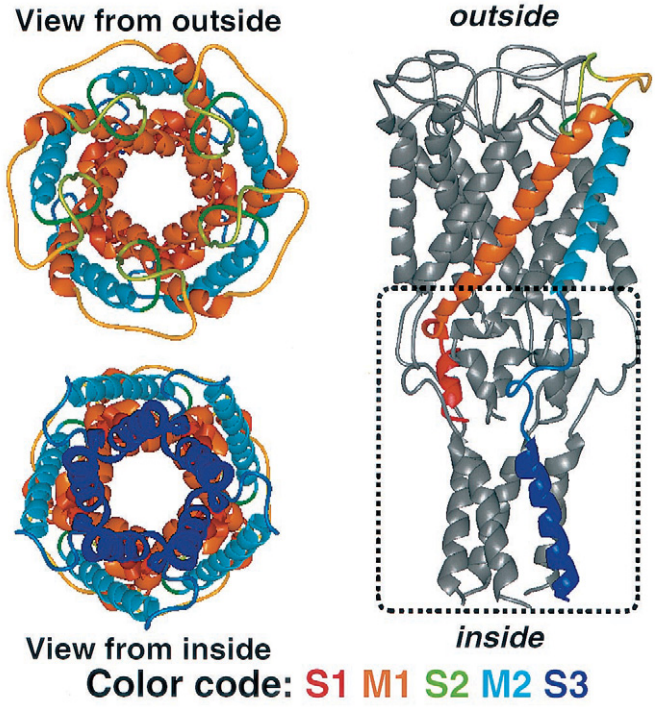


FIGURE 2 Ribbon representation of the backbone of a model of TbMscL in the closed conformation. View from outside the cell down the five-fold axis of the pore. Side view of the protein. In this model, the transmembrane helices, M1 (*orange*) and M2 (*cyan*), and periplasmic loop (*yellow* to *green*) are identical to the crystal structure (Chang et al., 1998). We have modeled the N-terminus S1 segment (*red*), which was unresolved in the crystal structure, to assemble as a bundle of amphipathic helices that blocks the cytoplasmic entrance to the pore. We have also modified the C-terminus S3 segment (*blue*) so that the loops from the M2 to S3 segments can accommodate the bundle of S1 helices. The S3 helices form a similar bundle of five helices in the crystal structure. The region of the model that does not correspond to the crystal structure is enclosed by the dashed line.

## RESULTS

### Model of TbMscL in the most closed conformation

Fig. 2 illustrates a pentameric model of the closed conformation of the *M. tuberculosis* MscL homolog. The transmembrane and extracellular regions were taken from the crystal structure (Chang et al., 1998). Each subunit contains two transmembrane $\alpha$-helices, M1 (*orange*) and M2 (*cyan*). The M1 helices are packed tightly together in the inner portion of the pore, forming the M1 gate, whereas the M2 helices are more peripheral. The red, S1, region represents the N-terminus segment that was unresolved in the crystal structure. In our models, S1 is postulated to form an amphipathic $\alpha$-helix because of its helical periodicity of strongly hydrophobic and strongly hydrophilic residues and because it is predicted to be helical by all secondary struc-

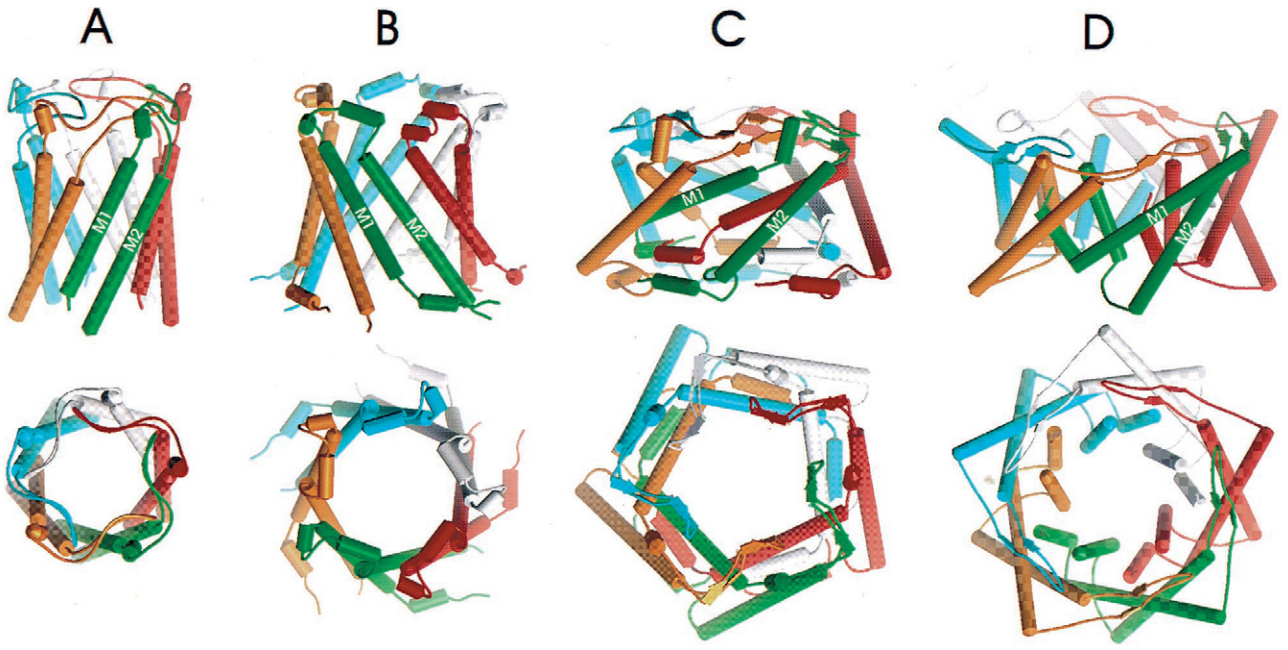


FIGURE 3 Alternative categories of models of the transmembrane region for the open conformation that we have considered. Cylinders represent $\alpha$-helices. Each subunit is colored differently. (*A*) The transmembrane region of this model differs from the closed conformation only by the position of M1. The outer C-terminus end of M1 has the same location as in the closed conformation, but the helix has swung away from the pore's axis so that the inner N-terminus is now located between the two adjacent M2s. (*B*) This model is similar to the first in that the pore is formed by both M1 and M2 throughout the transmembrane region; however, the two helices now tilt relative to the pore's axis in the opposite direction so that the helices pack together in a manner predicted by helix packing theories. (*C*) This model is similar to that of the closed conformation in that the inner portion of the pore is formed solely by M1 helices and the packing between M1 of one subunit and M2 of the adjacent subunit remains relatively unchanged. The conformational change involves increasing the tilts of both helices as they move radially away from the pore's axis. The S1, S2, and S3 segments are included because they are postulated to move into the transmembrane region to compensate for the shorter transmembrane distance spanned by the M1 and M2 helices. (*D*) In this model, the S1 and S3 amphipathic helices line the open pore, and the M1 and M2 helices form a cylindrical bundle that surrounds the M1-M2 bundle. The reasons that we favor the third category of models are described in the text.

ture prediction programs of the Pole Bio-informatique Lyonnalis site (http://pbil.ibcp.fr/cgi-bin/secpred consensus.pl). Five S1 helices are postulated to form a parallel bundle with 10 highly conserved phenylalanines (two per subunit) in its core. The S1 bundle plugs the pore from the inside, and is postulated to be the primary (S1) gate that does not open until the transmembrane region has expanded substantially. In the crystal structure, a highly conserved portion of the C-terminus, S3 (*blue*), forms an amphipathic $\alpha$-helix that self-aggregates to form a similar additional bundle of five parallel helices. We have modeled this region two ways: 1) as in the crystal structure and 2) with its highly conserved hydrophobic residues in the core of the bundle and the hydrophilic residues on the surface. The segment linking M2 to S2 has a relatively extended coiled structure in the crystal; however, the precise structure had to be modified in the model to accommodate the bundle of S1 helices. Although the precise structure of the C-terminus region in the closed conformation is ambiguous in our models, it is not a crucial feature, because the C-terminus is dispensable (Blount at al., 1996a). In both S1 and S3 bundles, the helices are tilted to form left-handed bundles in the manner typical of coiled-coil "knobs-into-holes" packing (Crick, 1953).

## The open conformation and general pathways for the gating transition

The first crucial issue in developing a model of the MscL gating mechanism is, "How does the in-plane area of the transmembrane region increase when tension induces the channel to open?" We have developed four categories of models for expanding the in-plane area and opening the transmembrane portion of the pore (see Fig. 3). In the closed crystal structure, the inner portion of the pore is formed solely by the five M1 helices. At the narrowest region, hydrophobic side chains on M1 pack closely enough together to present a barrier for the passage of ions. In the first two categories of models, the inner portion of the M1s is postulated to move away from the axis and lodge between the M2s so that the pore is lined by 10 helices (alternating M1s and M2s) throughout the transmembrane region. We call these the "10 helix pore" models. This type of model has been postulated previously by several groups (Chang et al., 1998; Blount and Moe, 1999; Batiza et al., 1999). The simplest version of a "10 helix pore" model is illustrated in Fig. 3 *A*. In this model the inner portion of M1 swings radially, with the inner portion moving much more than the

outer portion. The other segments remain similar to those of the crystal structure. The major drawbacks of this model are 1) a substantial number of hydrophobic residues of M2 are exposed to water in the pore; 2) the M1 and M2 helices in the first case pack next to each other in a manner that is not predicted by helix packing theory or that is frequently observed in membrane proteins; 3) the pore is smaller than suggested by experimental studies; 4) the periplasmic S2 loop is not strongly engaged in the conformational change, and thus the model does not explain effects on gating of modifications in the loop of EcoMscL (Blount et al., 1996b, Ajouz et al., 2000); and 5) numerous highly conserved residues do not interact with other conserved residues. Fig. 3 *B* illustrates another type of "10 helix pore" model with a larger pore and in which the helices are tilted in the opposite direction of the closed state so that all helices can pack next to each other with a crossing angle of ~10°, which is slightly less than typical of "coiled-coils," but more common type of helix packing between transmembrane helices (Bowie, 1997a). Although these models have some attractive features, the first and fifth drawback listed above are even worse in these models, and the transition pathway from the closed to open conformation is difficult to envision.

In the third category (Fig. 3 *C*), the inner portion of the pore is lined predominantly by the M1 helices in all conformations, and the expansion of the pore is caused by an increase in the tilt of the helices. We call these the "tilting 5 helix pore" models. Although this mechanism is less obvious, models of this type satisfy our modeling criteria better, provide a good explanation for many conserved aspects of the MscL sequences, and suggest how the transition from a closed to very large pore can occur without encountering large energy barriers. The change of water-accessible areas inside the pore among the closed, expanded, and fully open conformations is relatively small for this model because the pore becomes shorter as it becomes wider. Furthermore, many of the pore-lining residues are small, which allows polar backbone groups to contribute substantially to the lining. Thus, the estimated difference in hydration energies among the states is relatively small (4–7 kJ/mol or 1.6–3 *kT*). In contrast, in 10-helix models both M1 and M2 helices are "forced" to line the pore, with the latter uniformly hydrophobic in its cytoplasmic half. As a result, hydration of the inner surface of the pore depicted in Fig. 3 *B* may cost between 60 and 90 kJ/mol or 25–35 *kT*, making this structure highly unlikely. The major problem to be explained in 5-helix models is that the very tilted M1 and M2 helices cannot span the entire transmembrane region. The "flattened" open conformation may also distort the lipid bilayer around the channel due to the hydrophobic mismatch, which may bring one more term to the total energy of the open conformation. However, if tension makes the bilayer thinner, this may assist transition of the protein to a more flattened conformation (Andersen et al., 1999). For the more expanded conformations of these models, we postulate that hydrophobic faces of the periplasmic S2 domain and the cytoplasmic S3 helices interact with lipids at the surfaces to form a complete barrier between the lipids and the pore.

In the fourth category of models (Fig. 3 *D*), the pore is lined by a cylinder of 10 S1 and S3 amphipathic helices, which are surrounded by a cylinder of 10 M1 and M2 helices. Although these types of "10–10 helix pore models" satisfy most of our modeling criteria relatively well, experimental studies indicate that S3 is not an essential component of channel gating (Blount et al., 1996a), and the pore is smaller than suggested by experimental findings (see Discussion). The rest of this paper will focus primarily on "tilting 5-helix pore" models because they better satisfy our modeling criteria and are more consistent with experimental findings.

The second crucial question is, "What segment forms the gate?" If the gate is formed solely by a portion of the M1 helices, the mechanisms described above (see Chang et al., 1998; Yoshimura et al., 1999) would predict that rates of transitions between subconducting states should be tightly coupled to an increase of in-plane area of the channel complex. If so, then rates for each transition between substates should be highly tension-dependent, which is not supported by experimental observations (Sukharev et al., 1999). These findings suggest that another portion of the protein functions as a gate that is not tightly coupled to the in-plane area change during the initial expansion phase. The best candidates for an "uncoupled" gate are the N-terminal S1 helices that are capable of forming a bundle tightly associated with the cytoplasmic entrance to the pore. Other extramembranous segments are less likely candidates, as the C-terminal S3 domains are not critical for gating (Blount et al., 1996a), and the periplasmic S2 segments are poorly conserved among homologous sequences and in the TbMscL crystals do not occlude the pore.

In summary, we propose the following sequence of events leading to the opening in the wild-type MscL: 1) tension induces a substantial iris-like expansion of the transmembrane complex in which the tilt of M1 and M2 helices increases dramatically as they move radially away from the pore's axis; 2) hydrophobic surfaces of the S2 periplasmic loop and S3 helix move into the outer and inner lipid regions as the transmembrane distance spanned by the M1 and M2 helices decreases; 3) the S1-M1 linkers become fully stretched; 4) the pore opens as tension through the S1-M1 linker pulls the S1 bundle apart; 5) the individual S1 helices then dock on the perimeter of the complex. Details are specified below.

## Tension-induced changes in the barrel and the gating transition

We have developed models of TbMscL and EcoMscL in 13 conformations ranging from the most closed of the crystal structure to a conformation in which the narrowest part of the pore has a diameter of ~36 Å. Four of these

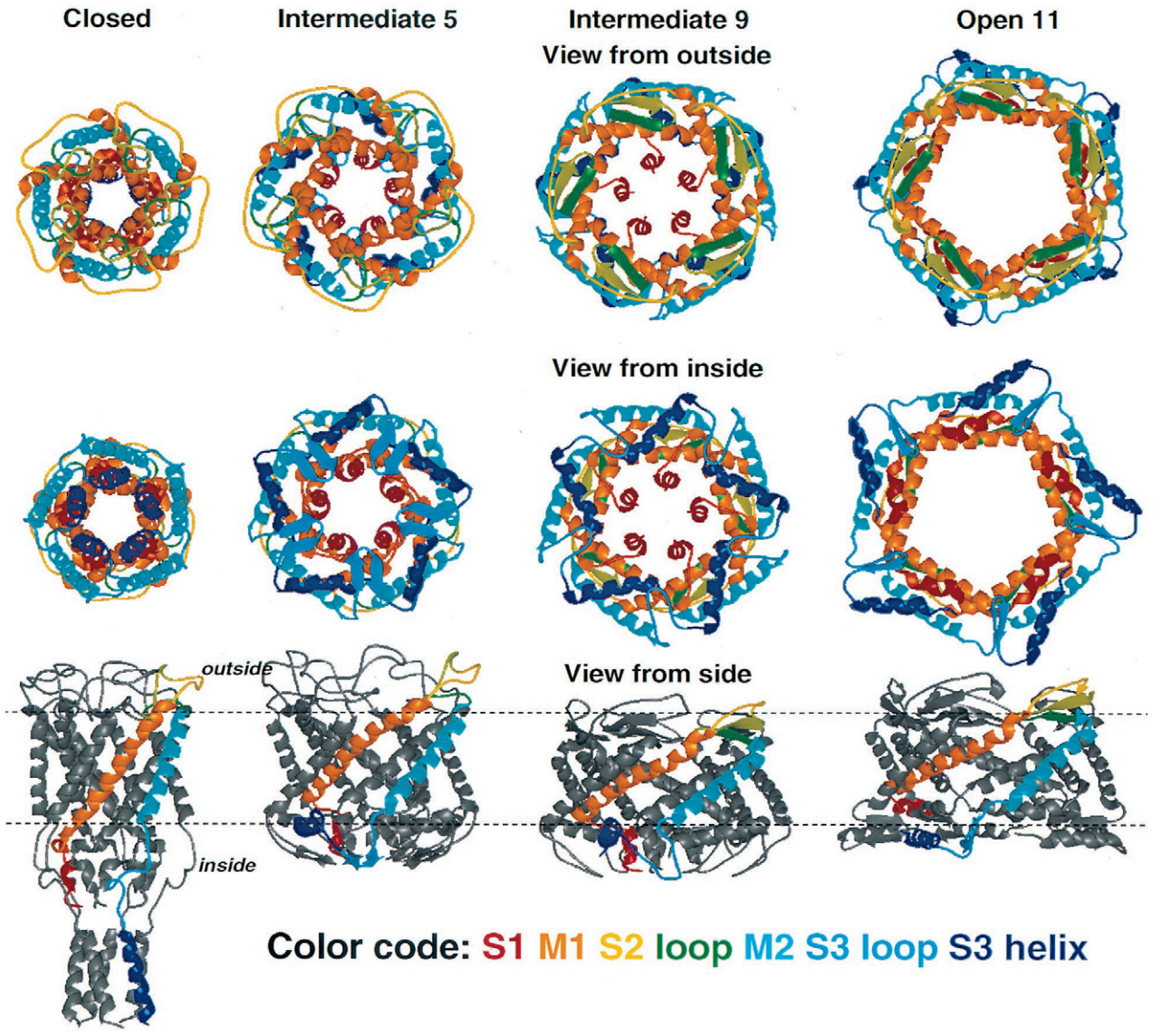


FIGURE 4 Ribbon representation of models of TbMscL in a closed, two intermediate, and an open conformations shown as viewed from outside the cell (*top row*), inside the cell (*middle*), and from the side (*bottom*). Only one subunit is colored in the side view, so that the conformation of a single subunit can be visualized. We have developed structural models of the MscL proteins in 13 different conformations of this category of models with different size transmembrane pores. Four of these conformations are illustrated here. The color code is the same as Fig. 2.

conformations for TbMscL are illustrated in Fig. 4. The transmembrane conformations selected in this paper to illustrate expanded but closed and open conformations are somewhat arbitrary because the exact points at which the S1 bundle will be pulled apart and at which the S1 helices will dock on the perimeter are difficult to predict. Of the 13 barrel conformations that we have modeled, conformation 11 is the largest for which the S1 helices can form the closed activation gate in the center of the complex without substantial distortion or unwinding of either the S1 or M2 helix and conformation 9 is the smallest that allows the channel to open with S1 binding to the postulated perimeter site on M1 and M2. In the TbMscL crystal structure, the M1 and M2 helices of adjacent subunits have a very large contact area, they are stabilized by van der Waals interactions, and their crossing angle is slightly positive (~10°), which is characteristic of "coiled-coil" type helix packing. We propose that the M1 and M2 of adjacent subunits stay together and change their tilt together as the barrel expands and becomes shorter. [However, during the final expansion steps the crossing angle may increase slightly in a manner that allows M2 to span more of the transmembrane region and that is nearer the optimal 20° crossing angle of "coiled-coil" type helix interactions.] M1 and M2 in the same subunit interact less intensively and, in our model,

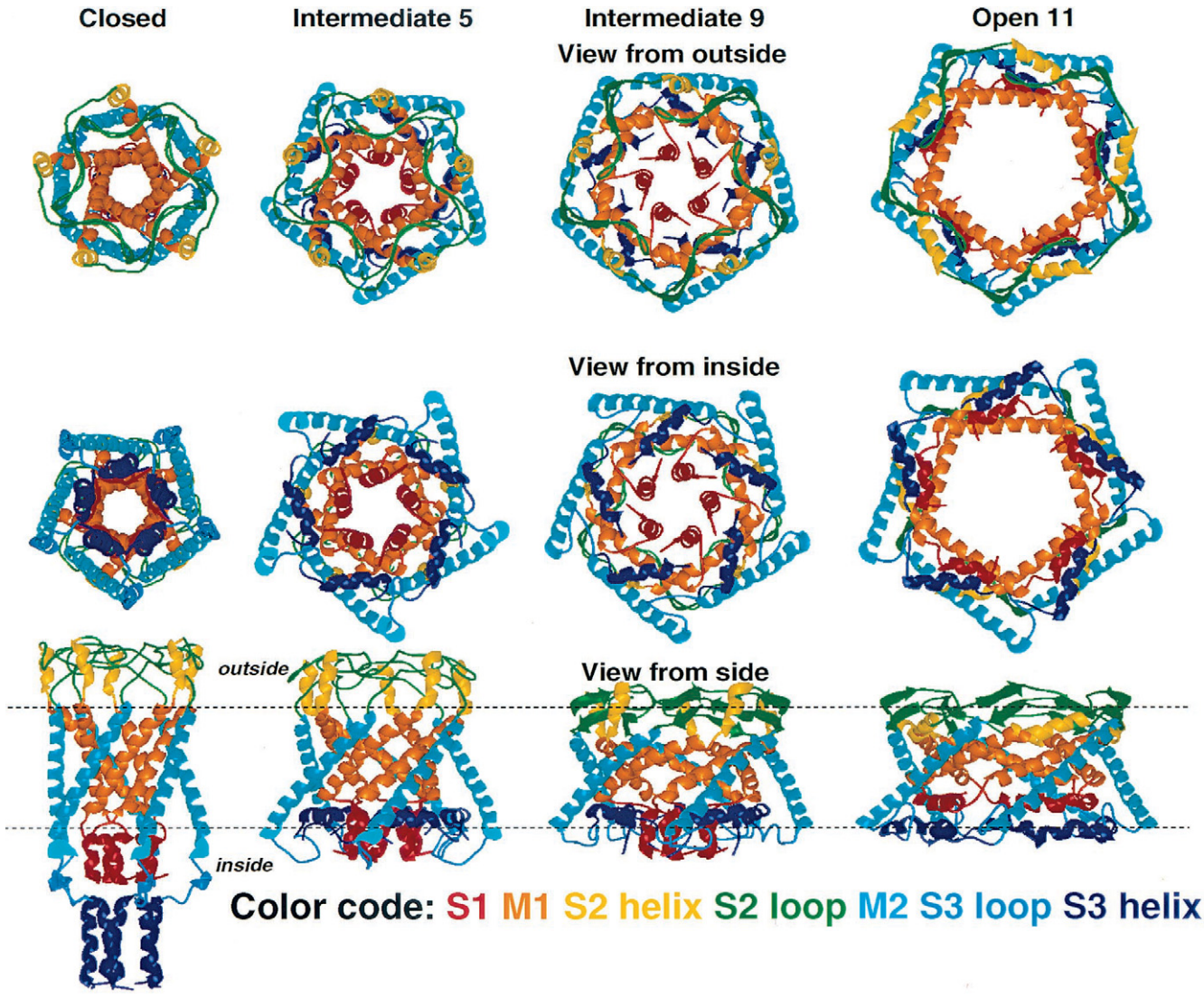


FIGURE 5 Similar to Fig. 4 but for EcoMscL. The primary differences between the backbones of TbMscL and EcoMscL are the conformations of the periplasmic S2 segment and the cytoplasmic segment linking M2 to the S3 helix. These segments are poorly conserved and bear little sequence similarity in the two models. They are also the most ambiguous portions of the models, and precise modeling is not necessary to postulate a basic mechanism common to all MscLs.

their relative position changes substantially as the barrel expands. This freedom is provided by changes in the periplasmic S2 loop conformation. As the periplasmic loop stretches from a coiled conformation to a primarily $\beta$ secondary structure, it moves into the outer lipid region, where it forms part of the outer wall of the pore, as described below. The tilts of helices change gradually for the 13 conformations and there are no substantial obstacles to the smooth sliding of the helices one along each other (as described later in the section on ridge-into-groove theory) even though the helices remain tightly packed with no substantial gaps. Analyses of membrane protein structures suggest that tyrosines and tryptophanes tend to anchor ends of transmembrane helices to the polar headgroup region (White and Wimley, 1999). MscL is atypical in that the M2 helix has only one tyrosine at the periplasmic end, and M1 has no tyrosines or tryptophanes near the headgroups. The absence of these anchoring residues may facilitate tilting of the helices.

We also developed similar models for EcoMscL, because most of the experimental data have been obtained for this protein. Backbone representations of four of these models are illustrated in Fig. 5. At this level, these models differ from those of TbMscL primarily in the periplasmic S2 loop and the loop connecting M2 to the S3 C-terminus $\alpha$-helix. These segments of the two proteins have virtually no sequence similarity. Details of the periplasmic loop models are described below.

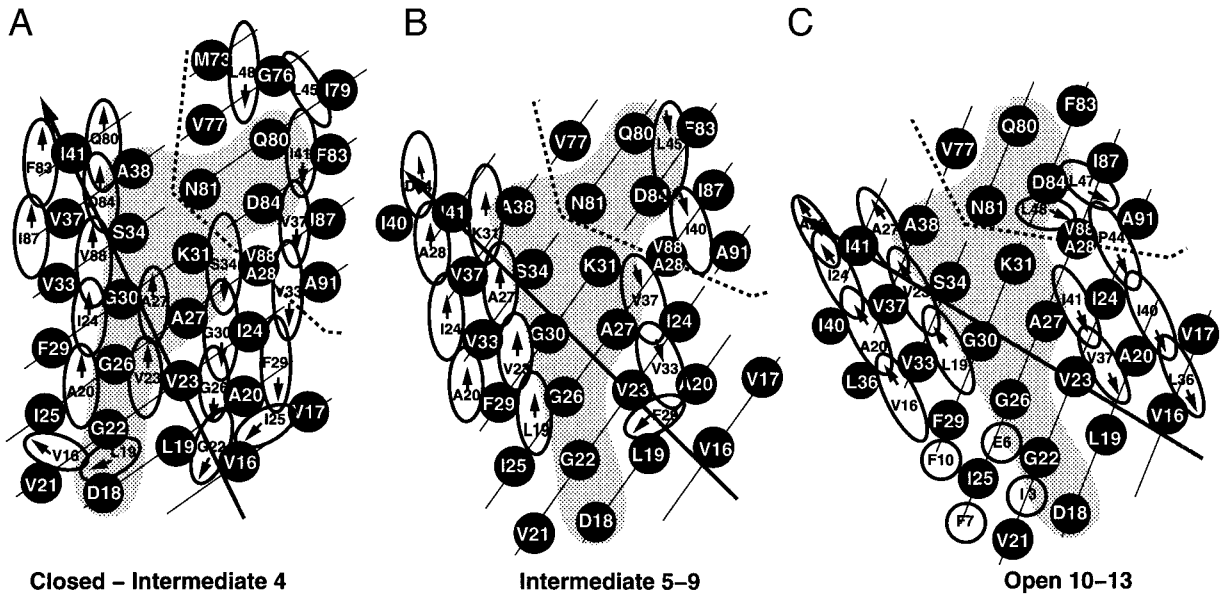


FIGURE 6 Helical net representation of how side chains of adjacent helices pack between each other for differ conformations as the size of the transmembrane helical bundle increases from conformation 1 (smallest closed) to conformation 13 (largest open). The black circles represent side chains of the central M1 and M2 (above dashed line) helices. The side chains are labeled with the one-letter amino acid code according to the EcoMscL sequence. The black lines through the circles represent the backbone and the gray arrow represents the axis of the central M1 and its tilt relative to the axis of the pore. Positions of side chains of M1s on each side of the central M1 helix are illustrated by the ellipses. The ellipses represent a series of conformations with the arrows within the ellipses indicating the direction of the movement of the side chains as the size of the pore increases. Note that the helices pack together according to "4–4 ridges-into-grooves" packing theory (Chothia et al., 1981) in which ridges formed by side chains that are four residues apart pack into the grooves formed between such ridges of the adjacent helix. This packing is maintained throughout the postulated movement except for the transition from the first to second net. The shaded region is composed of ambivalent and hydrophilic residues.

The iris-like movements of TM helices in both instances make the barrel wider and shorter. By the time the EcoMscL pore becomes 3 nm in diameter (7.5 $nm^2$ in cross-section) at the narrowest point to satisfy the observed unitary conductance (conformation 11), the average increase in the cross-sectional area of the protein complex reaches 22.7 $nm^2$, being 29.8 $nm^2$ at the cytoplasmic entrance, 17.7 $nm^2$ at the membrane midplane, and 20.8 $nm^2$ at the outer mouth of the channel. A simple thermodynamic analysis of dose-response curves has predicted an expansion of only 6.5 $nm^2$ for EcoMscL reconstituted in azolectin liposomes (Sukharev et al., 1999). This apparent discrepancy will be discussed below.

## The pore: ridges-into-grooves packing

The 4–4 ridges-into-grooves packing appears to be common for pore lining helices because it occurs between adjacent M1 helices in the crystal structure of TbMscL and between adjacent M2 helices of the KcsA potassium channel crystal structure (Rees et al., 2000; personal observation). In this packing mode, ridges formed by every fourth residue of one $\alpha$-helix fit into the grooves between similar ridges of an adjacent $\alpha$-helix. This pattern is illustrated for EcoMscL by a helix net representation in Fig. 6. (For a more detailed discussion of ridge-into-groove packing in proteins, see Appendix 2). In our postulated gating mechanism, this type of packing is maintained between the M1 helices throughout most of the very large conformational change; ridges cross over each other at only one point in this transition (corresponding to the transition from Fig. 6 *A* to *B*). All of the residues postulated to slide past each other are hydrophobic, thus avoiding breakage of H bonds during the conformational change. Application of this theory is made more reasonable by the relatively uniform nature of the interacting side chains; in the expanded conformations most of these are alkyl (Val, Ile, and Leu), which have similar volumes and atomic compositions. Two notable exceptions are A20 and F29, both of which are highly conserved. In our models the bulky F29 side chain passes over the small A20 side chain during the transition from Fig. 6 *A* to 6 *B*. In the open conformation A20 resides at the point of closest contact between adjacent M1 helices, while F29 interacts with F10 of the S1 segment (see Fig. 6 *C*). Sliding of the "ridges" along the "grooves" allows the helices to pack tightly next to each other without encountering large steric barriers during the transition.

## Residue polarity

We have developed these models so that most of the hydrophilic side-chain atoms are exposed to water and/or form H bonds, and most of the hydrophobic side chains are buried within the protein and/or exposed to lipid alkyl chains on the transmembrane surface of the protein. Ambivalent side

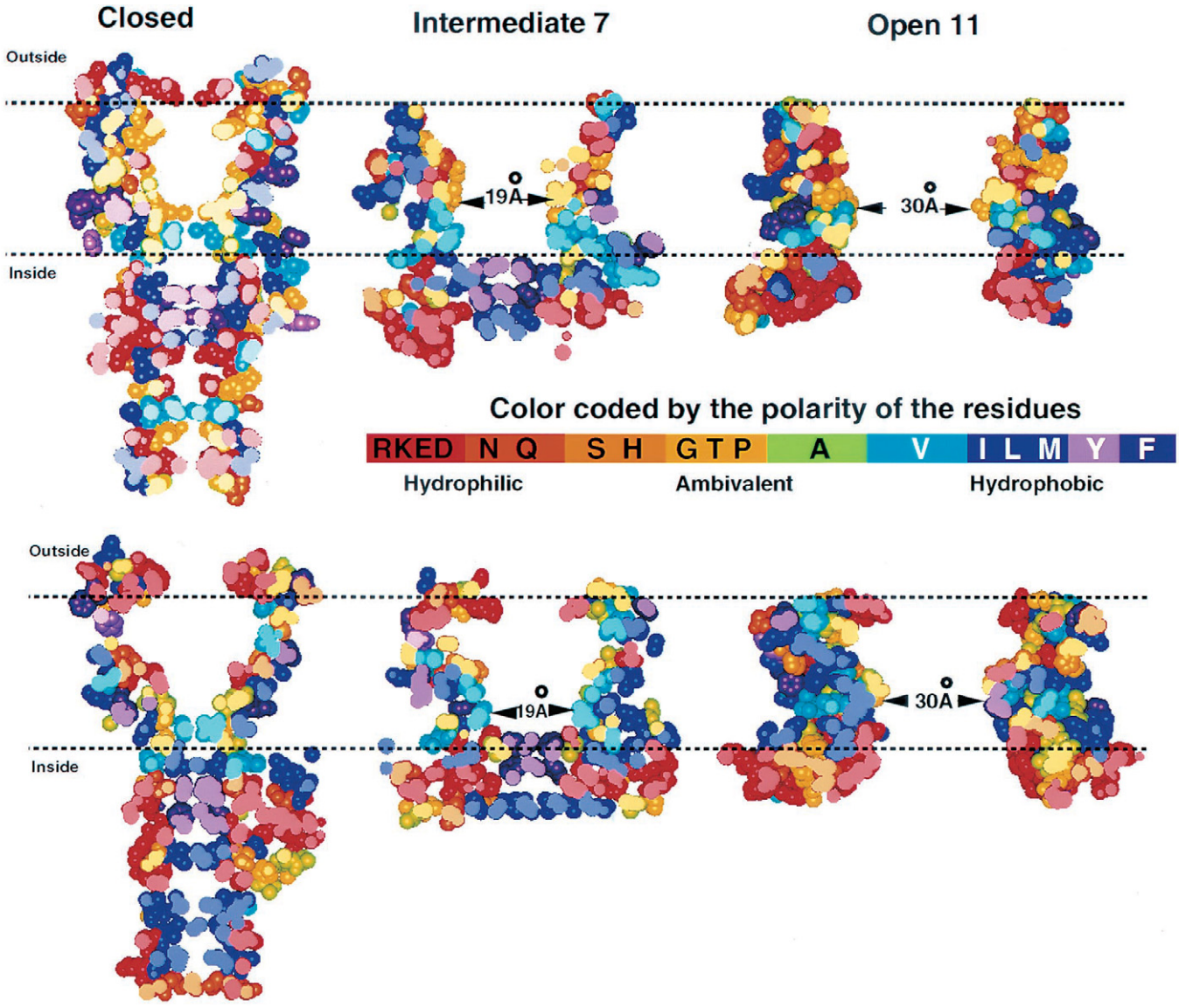


FIGURE 7 Side view cross-sections of space-filled models of TbMscL (*top*) and EcoMscL (*bottom*) in three conformations colored according to the residue's polarity. Note that most lipid-exposed residues are hydrophobic, most residues that are exposed to water in all conformations are hydrophilic, and most residues that are buried in some conformations and exposed to water in other conformations are ambivalent.

chains were permitted to be in any environment. [Ambivalent residues, A, G, C, S, T, H, and P, are defined here as those that are exposed or buried with almost equal probability in proteins of known structure (Guy, 1985; Miyazawa and Jernigan, 1999).] Fig. 6 illustrates that the M1 helix has one ridge formed exclusively of hydrophilic and ambivalent residues.

Fig. 7 illustrates that these criteria are satisfied reasonably well for three conformations of TbMscL and EcoMscL. In the closed conformation several ambivalent residues are buried, but they become exposed as the channel expands. The small size of the ambivalent residues allows polar backbone atoms to contribute to the pore's lining. A number of nonpolar side chains from residues V23, A27, V33, V37, and I41 are partially exposed to the pore in all conformations. However, as was mentioned above, the iris-like expansion of the barrel does not substantially change the total water-exposed area of M1 and M2 of EcoMscL. The polarity of the surface is balanced such that there is little change in energy related to hydration of the pore interior between conformations 1 and 9. In the smaller conformations, aliphatic side chains of L19 and V23 are exposed in the narrowest part of the pore. These may be to provide an additional hydrophobic barrier for ion permeation (M1 gate) and to repel water when the channel closes. In the expanded-closed intermediate conformations illustrated in Figs. 4, 5, and 7, we have repositioned the S3 amphipathic helices to the inner surface, where their hydrophobic residues interact

with hydrophobic residues of M1 and M2 and lipid alkyl chains, while their hydrophilic residues interact with the hydrophilic residues of the S1 helices and/or with water. This movement thus buries some hydrophobic residues on M1 and M2 that otherwise would be exposed to water in the pore, while it also helps compensate for the decrease in the hydrophobic region spanned by M1s and M2s. When the pore finally opens, the amphipathic S1 helices may interact with the same conserved hydrophobic residues of M1 and M2, and by docking to this site S1 may displace S3. This allows the S3 helices to move toward the cytoplasmic surface, where their hydrophobic residues may form an increased part of the outer wall of the protein that is in contact with alkyl chains of lipids. Thus, docking of S1s and possibly S3s on the perimeter should stabilize the expanded and open conformations by decreasing the hydrophobic surface area exposed to water in the pore and by increasing the hydrophobic surface area exposed to lipid alkyl chains on the protein's outer surface. Although it seems energetically favorable, the hypothesis that S3 docks at this site is very tentative, because EcoMscL gating doesn't substantially change after deletion of S3 (Blount et al., 1996a) and because there are no strong experimental results to support this hypothesis.

The loops are the most speculative portions of the models because they are quite variable among the different homologs, because there are no data regarding their structures for open channels, and because loops in general are difficult to model. Models of the S2 periplasmic loops for both TbMscL and EcoMscL were developed to make two points: 1) that S2 can accommodate in a structurally reasonable manner the large movement postulated to occur between M1 and M2 of the same subunit during gating, and 2) that the periplasmic loop may form part of the wall between the pore and lipid chains or headgroups when the channel is open. In the closed conformation, hydrophobic residues of the periplasmic loop, S2, tend to be buried in the core of the periplasmic domains (see Fig. 8). As the channel expands, these loops are postulated to change conformation in a manner that exposes the hydrophobic residues on the outer surface of the protein, where they make contact with lipid alkyl chains, while most of the hydrophilic residues extend into the pore, where they are exposed to water and where the charged residues form salt bridges. For TbMscL, the amount of secondary structure is postulated to increase, with the periplasmic region forming a triple-stranded $\beta$-sheet for the expanded conformations (Fig. 8 *A*). This is reasonable because regular secondary structure content of proteins and peptides often increases when they are moved from water to a more hydrophobic environment, and because segments of membrane proteins that are in contact with lipid alkyl chains almost always have a regular secondary structure. The sequence of the periplasmic loop in EcoMscL is so different from that of TbMscL that it was modeled in a different manner. In the model of Fig. 8 *B*, both open and closed conformations have a substantial amount of secondary structure, with the first part forming a short hydrophobic $\alpha$-helix and the latter part forming a distorted $\beta$ hairpin. In the closed conformation, the hydrophobic surface of the $\beta$ hairpin wraps around the more hydrophobic face of the helix. When the channel opens, the helix is pulled into the transmembrane region, leaving the hydrophobic surface of the $\beta$ hairpin exposed to lipid on the outer surface. Although details of these loop models are unlikely to be correct, they support the feasibility of the general hypotheses.

## Sequence conservation

Some of our modeling criteria depend upon analyzing the degree of sequence conservation at each position in an alignment of homologous proteins. Fig. 9 shows a sequence profile determined by aligning 36 MscL homologs. The homologs can be divided into subfamilies, the largest of which includes EcoMscL. The central line of Fig. 9 is the consensus (most frequently occurring residue) among the 13 sequences of the Eco-like subfamily. Letters above this line indicate other residues that occur at the analogous position within this subfamily. Letters below the line indicate residue types that do not occur within the Eco-like subfamily, but that do occur in more distantly related homologs. The alignments of distantly related sequences for segments linking M1 to M2 and M2 to the S3 helix are ambiguous, and thus letters below the line for these segments should be taken only as an indication of the high degree of sequence variation. We have used data for the entire family only for those residues that are well conserved within the family; i.e., those residues that are colored red, orange, and yellow in Fig. 9. These residues are all within segments that can be aligned unambiguously for the entire superfamily. The remaining residues were scored according to their degree of sequence identity within the Eco-like subfamily, which can be aligned unambiguously for all residues. Fig. 9 illustrates that there are two strong general regions of conservation within the family: the latter portion of S1 through the first half of M1 and S3.

Fig. 10 illustrates space-filled models of three putative conformations of the EcoMscL in which the residues are colored according their degree of sequence conservation. In the closed conformation, the more highly conserved residues are strung out along the axis of 5-fold symmetry in the cytoplasm and inner part of the transmembrane region. These residues in S1 and M2 include those that occlude the closed pore. In the intermediate conformation, the conserved residues of M1 and M2 have moved away from the axis, while conserved residues on S1 and S3 have moved nearer the transmembrane segments to form a complex with a highly conserved core on the cytoplasmic surface of the membrane. Note that in the fifth to seventh radial cross-sections, residues on the radially outer surface of the complex tend to be poorly conserved. Residues in the other

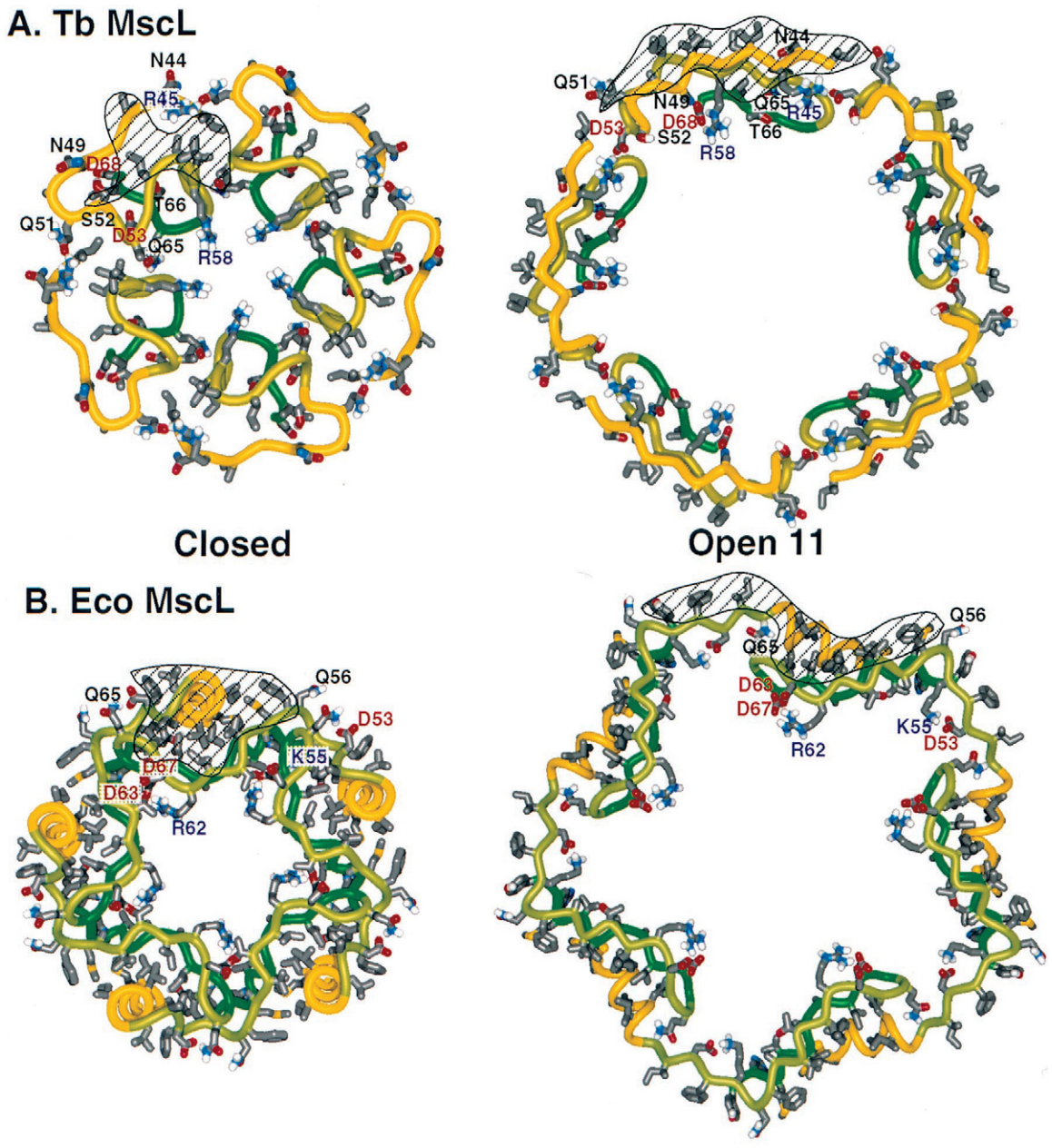


FIGURE 8 Models of the periplasmic S2 loops in the most closed and open conformations. (*A*) The closed conformation for TbMscL is that of the crystal structure (Chang et al., 1998). The open conformation was model so that the S2 loop could connect M1 to M2 in a way that allows its hydrophobic residues to interact with lipid chains on the exterior of the protein while its hydrophilic residues extend into the pore and its charged side chain groups form salt bridges. Most of the backbone forms a triple-stranded $\beta$-sheet. (*B*) The EcoMscL S2 segment was modeled so that the first part forms a short $\alpha$-helix and the remaining portion forms a distorted $\beta$ hairpin. In the closed conformation, the hydrophobic residues of the $\beta$ hairpin interact with those of the helix to form a hydrophobic core (see shaded region). In the open conformation, the hydrophobic helix is pulled into the outer portion of the transmembrane region, and the hydrophobic face of the $\beta$ hairpin comes into contact with the surrounding lipid (not shown). The side chains are colored by atom type; gray = carbon, red = oxygen, blue = nitrogen. Some of the hydrophilic residues are labeled.

cross-sections are not as cleanly segregated into highly conserved core residue and poorly conserved surface residues, perhaps because the pore is so large in all conformations for the outer cross-sections that pore-lining residues can be considered to be water-exposed surface residues. Nonetheless, conserved residues in these regions still have a tendency to cluster together, as indicated by the yellow clusters in the first and second cross-sections. When the channel opens, no residues are on the radial axis of the protein, and highly conserved residues tend to form clusters in the walls in all of the radial cross-sections (Fig. 10, *bottom*).

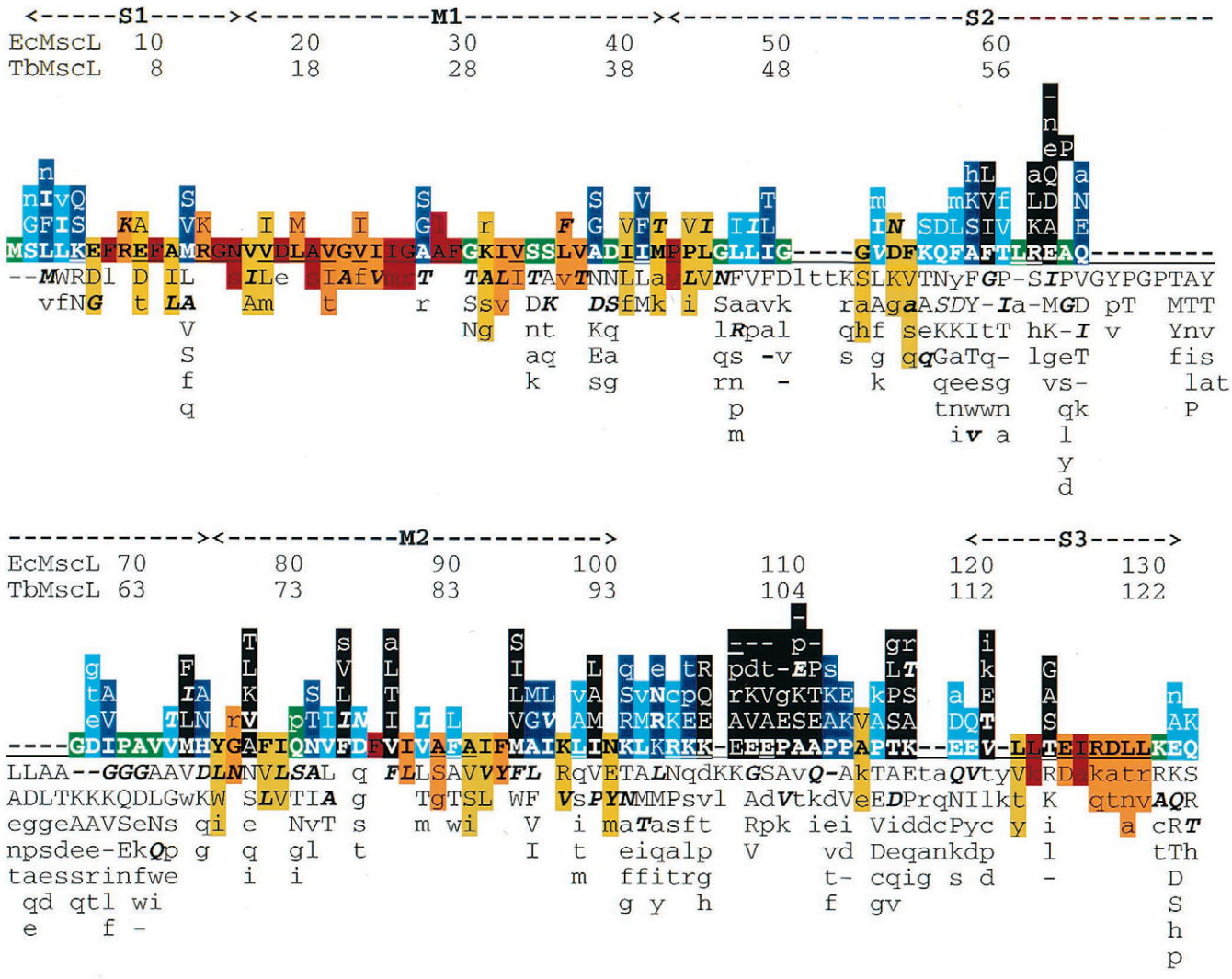


FIGURE 9 Consensus sequence of the *E. coli*-like subfamily (*central line*) and other residues that occur at the same location within the MscL superfamily. Letters above the central line indicate additional residues that occur within the *E. coli*-like subfamily and those below the line indicate residue types that do not occur within the *E. coli*-like subfamily but that do occur in more distantly related MscL sequences. Lowercase letters indicate that the residue type occurs in only one MscL sequence. The residues are colored according to the degree of sequence conservation within the entire superfamily for the more highly conserved residues or within the *E. coli*-like subfamily for less well-conserved residues. To calculate the degree of conservation at each position, uppercase letters were given a score of 1 and lowercase a score of 0.5. The color code for the more highly conserved residues is red = 1–1.5, orange = 2–2.5, and yellow = 3–3.5, with all residues of the superfamily counted. For the remaining residues, only those residues within the *E. coli*-like subfamily were counted: green = 1–1.5, cyan = 2–2.5, blue = 3–3.5, and black = 4 or more. The sources for the sequence are listed in Appendix 1. The EcoMscL sequence is in bold type; the TbMscL sequence is bold and italicized.

The models provide an explanation for the structural or functional role of the highly conserved segments and residues. The amphipathic nature of the S1 and S3 helices is important for formation of the cytoplasmic gate of the closed conformations and of the inner portion of the channel's wall of the open conformation. When the channel is open, S1 forms part of the inner pore lining, with its hydrophobic face interacting with hydrophobic surfaces of M1 and M2 while its hydrophilic face interacts with water in the pore and cytoplasm and with the hydrophilic face of S3. S3 is more peripheral and may form part of the lipid-exposed wall on the cytoplasmic surface with its hydrophobic residues interacting with lipid alkyl chains and its hydrophilic face interacting with water of the cytoplasm, polar residues of S1, and lipid headgroups. Although the activation gate is formed by S1 segments in our models, tight packing of the inner portions of the M1 segments (M1 gate), as occurs in the crystal structure, appears to be important for insuring that the channel does not leak at rest (see Discussion). The hydrophobic constriction in the closed pore made by conserved L19 and V23 (in EcoMscL) not only pose a hydrophobic barrier to ion permeation (M1 gate), but also may

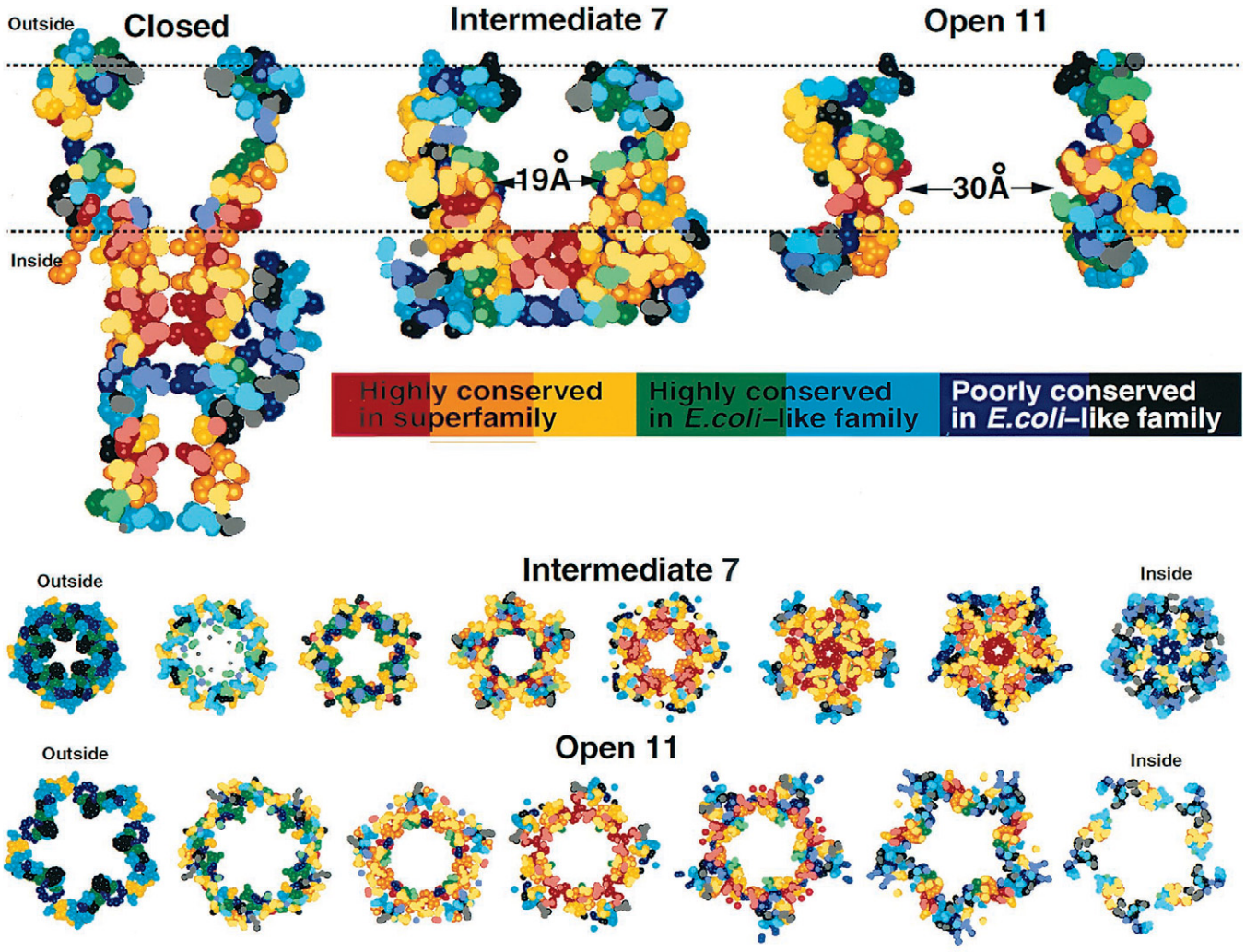


FIGURE 10 Space-filled models of EcoMscL in three conformations colored by extent of sequence conservation. Side view of three conformations. Serial cross-sections (6 Å thick) for conformations 7 and 11, beginning with the periplasmic side. Note that for all conformations, most highly conserved residues interact with other highly conserved residues and most poorly conserved residues are on the protein's surface. The color code is the same as in Fig. 9.

assist fast expulsion of water when the pore returns from the fully hydrated open to the closed state. Several of the highly conserved residues of the inner portion of M1 residues are ambivalent. The ability of these residues to reside almost equally well in either a hydrophobic or hydrophilic environment may be important because they tend to be buried in the most closed or resting conformation, but become exposed to water during the expansion phase. Their small size is also important for allowing tight packing of the M1 helices of the closed conformation. The periplasmic loops have numerous hydrophobic residues. This hydrophobicity may be important for gating if, as proposed here, their hydrophobic side chains interact with lipids at the outer membrane surface when the channel opens. The extensive number of complementary interactions, e.g., salt bridging, H bonding, aromatic-aromatic, and hydrophobic-hydrophobic, among the highly conserved residues of these models, satisfies our homology modeling criteria quite well. A detailed list of the interactions among highly conserved residues is given in Table 1. The MscL family of sequences has five highly conserved phenylalanines. For the closed conformations F7 and F10 residues of all five EcoMscL S1 segments interact with each other to form the core of the gate that occludes the pore. When the channel opens, S1 moves to the perimeter where F7 interacts with F93 of M2 and F10 docks between F29 of M1 and F85 of M2. Salt bridges are also energetically favorable, and in our model almost all of the charged side chain groups form salt bridges. Some of these are highly conserved. In almost all of our models, R13 at the end of S1 binds to D18 near the beginning of M1; D18 also binds to the N-terminus of S1 for the open conformations. In the expanded intermediate conformations and open conformations, R8 and E9 of S1 bind to D127 and R126 of S3. Glycine has more conforma-

**TABLE 1 Interactions with highly conserved residues for three different conformations of EcoMscL**

| Residue | Closed Conformation | Intermediate Conformation 7 | Open Conformation 11 |
|---|---|---|---|
| e6 | **F7**, R8, & N-terminus amine | **F7**, R8, *k130*, & N-terminus amine | G22, **I25**, **G26**, & N-terminus amine. Pore |
| **F7** | *i3*, e6, 2 **F7**'s & **F10**, Blocks | *i3*, e6, 2 **F7**'s & **F10** Blocks | A89, i92, F93, i96, & L129 |
| R8 | e6, *e107* | e6, D127, *k130, e131*, & *q132* | R126, D127, L129, *k130*, & *e131*. Pore |
| e9 | a11, R13, *k106* | a11, R13, R126, *k130* | R126 and *k130*. Pore |
| **F10** | **F7**, 2 **F10**'s, **N15**, **D18**, & 2 L19, Blocks | **F7**, 2 **F10**'s, a11, & R13. Blocks | **G14**, **I25**, **A28**, **F29**, I32, **F85**, A89, & i92 |
| a11 | e9, r13, **N15** | e9, **F10**, & R13. | **I125**, R125, & L129 |
| R13 | e9, a11, **G14**, **N15**, V17, **D18**, n100, & C-terminus of S1 | e9, **F10**, a11, **D18**, L19, & **I25** | **D18**. Pore |
| **G14** | e9, R13, **D18**, & v16 | e9, L19, **I25**, **L122**, **I125**, & R126 | **F10** & **F29**. Pore |
| **N15** | e9, **F10**, R13, **D18**, & C-termini of S1. | **D18**, **L122**, *e118, e119*, R126, & N-terminus of M1 | N-terminus of M1 |
| v16 | **G14**, **D18**, V21, G22, & i96 | **F29**, **F85**, **L122**, & *e119* | L36 & f78 |
| v17 | R13, G22, i96, & *i99* | I96, *i99* & L129 | I32, i40, lipid |
| ***D18*** | **F10**, R13, **G14**, **N15**, v16, L19, & N-terminus of adjacent M1 helix | **R13**, **N15**, R126, L129, & *k117* | R13 & N-terminus of S1 |
| L19 | 2 **F10**'s, 2 L19's, & **D18**. Blocks | R13, **G14**, **I25**, **F29**, & **F85** | **G14**, **F29**, & V33 |
| **A20** | G22, **G26**, **I25**, & **G25** | **F29** | V33, L36, V37, & i40 |
| V21 | i92 & i96 | i92, **I125**, L128, & L129 | *i3*, i40, & i92 |
| G22 | v17, L19, & **A20** | *m12* & L129. Pore | *m1, i3*, & e6 |
| V23 | 2 V23's, & **G26**. Blocks | **F29**, g30, & V33. Pore | *m1*, V33, & V37. Pore |
| I24 | **G26**, **F29**, i92, & *v88* | V33, L36, V37, *v88*, & i92 | V37, i40, *i41*, p44 |
| **I25** | **A20**, **F85**, *v88*, A89, i92 & F93 | R13, L19, **F85**, *v88*, i92, & **I125** | *i3*, e6, **F7**, **F10**, i92 |
| **G26** | **A20**, V23, & I24 | R13. Pore | e6. Pore |
| **A28** | **F85** & *v88* | V37, *v88* | **F10**, **F85**, & *v88* |
| **F29** | I24, **F85**, I87, *v88*, & a91 | v16, L19, **A20**, V23, & **F85** | **F10**, **G14**, & L19. Pore |
| k31 | *s34, q80, n81*, & *d84* | *i41, q80, n81*, & *d84* | *Q80, n81*, & *d84*. Pore |
| I32 | *n81* & **F85** | *n81* & **F85** | **F10**, v16, n81, & **F85** |
| V33 | *d84*, I87, & *v88* | V23, I24, & *a27* | L19, **A20**, & V23. Pore |
| L36 | f78 & *n81* | I24, f78, & *n81* | V16, **A20**, f78, *n81* |
| V37 | *q80, f83, d84*, & I87 | I24, *a27*, & **A28** | **A20**, V23, I24. Pore |
| i40 | m42, f78, & lipid | f78, I87, & *v88* | v16, v17, **A20**, V21, I24 |
| m42 | *d39*, i40, & 145 | *m73* & lipid | *v71, v72*, & *m73* |
| **P43** | f54 & lipid | lipid | Lipid |
| p44 | f54, k55, *i68*, & y75 | *q80* | I24 |
| 145 | ***m42***, *i68, v71*, & *v72* | *v71, v72*, & *m73* | *p69, a79*, & *v71* |
| g51 | Periplasm | *a64* & *l61* | *q80* & *f83* |
| d53 | *l47* & *q65* | *l47, k55*, & y75 | G76 & *q80*. Pore |
| f54 | **P43**, p44, & y75 | *l47* & y75 | y75, G76, & I79 |
| y75 | p44, f54, & *i41* | f54, *k55*, & d53 | f54, *k55*, & *q56* |
| G76 | Lipid, N-cap for helix M2 | Lipid headgroup, N-cap for helix M2 | d53 & f54. Lipid. N-cap for helix M2 |
| f78 | L36, *d39*, & i40 | L36, *d39*, & i40 | v16 & L36. Lipid |
| i79 | Lipid | Lipid | *i52* & f54. Lipid |
| **F85** | **I25**, **A28**, **F29**, & I32 | v16, L19, **I25**, **A28**, & **F29** | **F10** & I32 |
| I87 | **F29**, I33, & v37 | i40 & lipid | *l47*. Lipid |
| A89 | **I25** & lipid | 1121, **L122**, & **I125** | **F7** |
| a91 | **F29** | Lipid | Lipid |
| i92 | V21, I24, & **I25** | V21, I24, **I25** & **I125** | I3, **F7**, **F10**, V21, **I25** |
| F93 | **I25** & lipid | L121, E124, & **I125** | **F7** & L129 |
| i96 | R13, v16, v17, & V21 | E124, **I125**, & L128 | *i3*, i4, & **F7** |
| k97 | Lipid headgroups | E124 | *q132* & Lipid headgroups |
| n100 | R13 & C-terminus of S1 | *r104, e108, a111, a113*, & *p113* | *q132* & *n133* |
| l121 | 2 l121's, **L122**, & **I125** | A89 & F93 | *m12* & Lipid |
| **L122** | *K117, v120*, L121, & E124 | **G14**, **N15**, V16, **F85**, & A89 | *m12* & R13 |
| E124 | **L122**, **I125**, & R126 | F93, k97 | Cytoplasm |
| **I125** | l121, 2 **I125**'s, E124, & L128 | **G14**, V21, **I25**, I92, F93, & i96 | a11 & *m12* |
| R126 | E124 & D127 | e9, **N15**, **D18** & *e118* | R8, e9, & D127. Pore |
| D127 | R126 & L129 | R8 | R8 & R126. Pore |
| L128 | 2 L128's & L129 | V17, V21, i96, & *p113* | Lipid |
| L129 | D127 & L128 | *m12*, R13, **D18**, V21, & G22 | **F7**, R8, a11, & F93 |

Code: **Bold uppercase**, **most highly conserved**; uppercase, second-best conserved; lowercase, third-best conserved; *Italics*, *not conserved*.

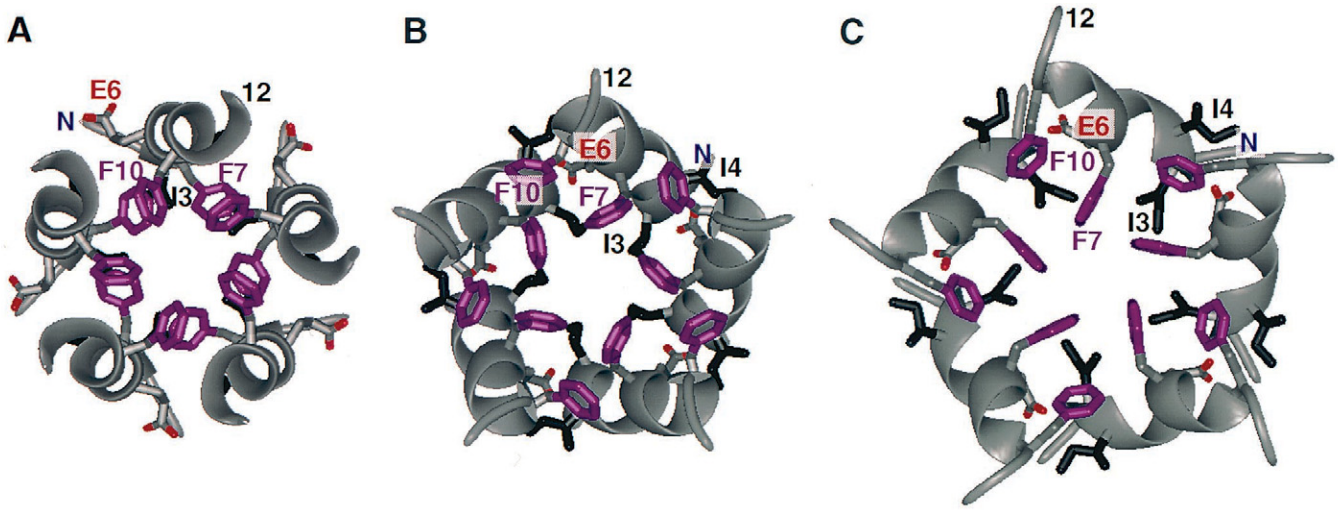


FIGURE 11 Models of the S1 bundles as viewed from the extracellular side looking through the pore. (*A*) A tightly packed left-handed bundle used for the more tightly closed conformations. (*B*) A right-handed bundle used for expanded-closed conformation. (*C*) A very tilted right-handed bundle used for the most expanded-closed conformation. Hydrophobic phenylalanine (*purple*) and isoleucine (*black*) side chains are shown. The Glu-6 side chain (*red*) binds to the N-terminus (*blue N*) in the right-handed bundles. Note that in *B* and *C* the F10 side chain from one subunit interacts with the I3, I4, and F7 of the adjacent subunit.

tional freedom than other residues. Thus, the reason that G14 of the S1-M1 linker is absolutely conserved may be related to the flexibility of this segment, which changes conformation throughout the expansion and opening transitions in our models. A20 is one of the most highly conserved residues in M1. In our models, the equally conserved and bulky F29 residue moves over the small A20 during the expansion phase, and A20 forms the closest contact between adjacent M1 helices in the open conformations, thus facilitating tight packing of the helices.

### Substates

As the channel barrel expands and the linkers start pulling on the S1 gate, the tight left-handed S1 bundle with typical coiled-coiled packing may switch to right-handed conformations in which the ends of the helices are farther from the axis of the pore, as illustrated in Fig. 11. The helices of the right-handed bundle pack more similarly to those of the M1 helices in MscL and the M2 helices in the KcsA potassium channel. Currently, we cannot answer the question of whether one of these expanded conformations is leaky and represents one of the low-conducting substates that is stable in several gain-of-function mutants (Yoshimura et al., 1999). Alternatively, the transition from the closed-expanded conformation to the first substate may occur when one S1 helix moves to the perimeter of the structure. Thus, the substates of Fig. 1 represent semi-open conformations in which the bundle of five S1 helices has been partially disrupted but not all of the S1 helices have docked into their binding sites on the perimeter of the structure. Thermodynamic analysis of MscL reconstituted in liposomes suggested that formation of the first substate involves about 4 $nm^2$ expansion of the transmembrane pore; however, further transitions from the first substate to the fully open conformation are associated together with a lesser expansion of ~2 $nm^2$. The actual process of the breakdown of the activation gate and formation of the fully open channel is difficult to model precisely because it is likely to be a highly dynamic process with numerous pathways and transient conformations.

## DISCUSSION

Direct experimental evaluation of our models of EcoMscL is currently under way, and part of it has been published recently (Sukharev et al., 2001). By using single and double cysteine substitutions, disulfide trapping, and patch-clamp recording in the presence of oxidizing and reducing agents we have been able to support the following general model predictions.

First, the S1 domains form a bundle that occludes the pore from the cytoplasmic side. Indeed, disulfide bridges spontaneously cross-link adjacent subunits for F7C and F10C mutants. These bridges prevent the channel from complete opening under any pressure. The F7C and F10C disulfide bridges can be reduced, and this results in channel activation. Both are reduced more readily by mercaptoethanol in the pipette rather than in the cytoplasm, which is consistent with our model in which F10 residues should be at the bottom of the pore, where they should be more readily

accessible through the pore than the cytoplasm. Disulfide bridges rarely form spontaneously in cysteine mutants; e.g., none has been observed for KcsA mutants even though many of the mutated residues are near the fourfold axis of symmetry (E. Perozo, personal communication). Thus, when they do form, it likely indicates that the residues are near each other in the native structure. The I3C mutant forms disulfide bridges when exposed to the oxidizing reagent iodine. After exposure to iodine, the I3C channel can open only to subconducting states (Sukharev et al., 2001). This result is less compelling than those for the F7C and F10C mutants because, when oxidizing reagents are present, residues that are distant in crystal structures can sometimes form disulfide bridges when mutated to cysteine (Butler and Falke, 1996). The observation that these mutants can still gate to subconductance states does suggest that formation of the disulfide bridge(s) has not altered the protein's structure dramatically.

Second, when the S1 bundle breaks apart, leading to the fully open conformation, individual S1 helices may dock to a specific site on the inner surface of the pore. I3 on S1 and I96 on M2 of a different subunit are predicted to pack close to each other in this conformation. Patch-clamp experiments demonstrated that when the I3C/I96C double mutant is exposed to iodine in the pipette with suction applied to open the channel, the channel gates predominantly between the fully open state and one of the substates, and rarely closes completely. This behavior indicates that a disulfide bridge can form between I3C and I96C, immobilizing one or several gate segments in the open conformation (Sukharev et al., 2001). The fact that open channels form in these mutants supports the postulation that these residues are proximal in normal open channels, and strongly suggests that some of the subconducting states reflect the dynamics of S1 domains.

Third, when membrane tension stretches the transmembrane (TM) region, the tilts of the TM helices increase. We have evidence for disulfide coupling between residues A20C and L36C, which can be obtained only under conditions of osmotic shock in the presence of oxidizing agent (M. Betanzos, C.-S. Chiang, H. R. Guy, and S. Sukharev, manuscript in preparation). The proximity of these residues is possible only if adjacent M1 helices are tilted to ~65–70°, reaching conformation 9 or 10 (see Fig. 5). Alternative 10-helix models of the open conformation predict that A20 and L36 should be very far apart because M1 helices of adjacent subunits should be separated by M2 helices and A20 should be near the cytoplasmic entrance, while L36 should be near the periplasmic entrance.

Fourth, according to the model, the length of the S1-M1 linker (R13-G14-N15 in EcoMscL) is critical for channel gating. The linker may be slack in the resting closed conformation, but it must transmit the stretch to S1 gates when the barrel is expanded beyond a certain point. The shorter linker would render the channel hypersensitive to stretch or prevent complete closure. Conversely, if it is too long, the deformation of the barrel to its very limit may not result in sufficient stress in linkers, and the channel could remain closed at any tension. The length of the S1-M1 linker is conspicuously preserved in all 36 species. The EcoMscL mutant with deleted G14 (ΔG14) was reported to lock spontaneously in the low subconducting state and remain in this state in the absence of mechanical stimulus (Liu et al., 1999). Insertion of extra glycine next to G14 (double G14 mutation) results in the channel that activates almost normally, but preferentially occupies lower subconductances, indicating that longer linkers provide more freedom for S1s to recombine into partially closed conformation (Sukharev et al., 2001). Insertion of a GAG sequence instead of G14 (extending the linker with two extra residues) creates a channel that barely opens and then irreversibly inactivates (Sukharev et al., 2001). These findings support our postulate that the S1-M1 linker serves as a "string," linking expanding transmembrane segments (M1s) to the gate (S1s).

The models presented here are also consistent with most of the experimental findings regarding the conductance, kinetics, and mechanosensitivity of the native MscL channel and many mutants.

## The size of the pore

EcoMscL has no selectivity and its conductance is strictly proportional to the conductivity of the bulk electrolyte in a wide range of salt concentrations. The conducting properties of the solution in the pore thus seem to be similar to those in the bulk, suggesting a wide aqueous pore. There are few unbalanced charges in the pore or near the entrance, consistent with indiscriminate passage of anions and cations (Sukharev et al., 1994). The pore diameter estimated from single-channel conductance using the method of Hille (1992) is between 2.9 and 3.5 nm, if the length of the pore is estimated to be 3 to 5 nm (Sukharev et al., 1999). Independently, the MscL conductance measurements in the presence of poly-L-lysines of different sizes suggested the pore of ~4.0 nm (Cruickshank et al., 1997). Many intracellular components, such as amino acids (Britten and McClure, 1962), sugars, and nucleotides leave the cell during osmotic shock and may pass through the open channel. It has been proposed that osmotic shock-sensitive release of thioredoxin (Ajouz et al., 1998), EF-Tu, and DnaK (Berrier et al., 2000) also takes place through MscL. These results are not fully consistent with our models. Thioredoxin may pass only through the most expanded barrel (conformation 13), whereas EF-Tu and DnaK appear to be too large and would have to unfold to pass through even the largest pore conformation that we have modeled. However, a recent study finds that passage of these proteins through the membrane does not involve MscL (Vazquez-Laslop et al., 2001). The diameter of the narrowest region of the open pore in our models ranges from 3.0 to 3.7 nm. For the models that we propose, expansion of the pore diameter beyond 3.7 nm either creates gaps in the pore lining or does not allow adjacent M1 helices to overlap, either of which we consider unlikely.

## Barrel expansion

The models illustrate that an "elastic" deformation of the barrel is plausible. While examining numerous sequential conformations with gradually increasing tilts of M1 and M2 domains, we have not encountered any substantial steric obstacles. The process of MscL expansion accompanied with flattening of the transmembrane barrel has been recently simulated by virtual molecular dynamic experiments (Gullingsrud et al., 2001). The sliding of helices predicts smooth transitions through the continuum of closed conformations until the transition barrier is reached. This is consistent with typical single-mode closed time distributions observed in single-channel patches (Chiang, Anishkin, and Sukharev, manuscript in preparation). A two-state kinetic analysis of MscL in liposome patches suggested that the transition barrier is slightly shifted toward the center of the open state well, making the closed conformation more compliant ("soft") compared to the open conformation (Sukharev et al., 1999).

An apparent discrepancy has arisen regarding the amount of channel expansion, $\Delta A$, associated with the opening. Our models built to satisfy conducting properties of the open channel predict a 7 $nm^2$ cross-sectional area of the water-filled pore and 22.7 $nm^2$ for total expansion, whereas the steepness of the tension-dependency for open probability in azolectin liposomes predicted only 6.5 $nm^2$ for total expansion. We are more confident in model predictions based on the physical size of the open channel. In contrast to the earlier gating data obtained in soybean lipids (Sukharev et al. 1999), more recent measurements in spheroplasts produced estimates of $\Delta A$ of $\sim$19 $nm^2$ (Chiang and Sukharev, unpublished observations), which are more consistent with the model. Therefore, the foreign lipid environment may somehow modify the path for the transition, allowing the channel to expand silently (i.e., without opening) for $\sim$14 $nm^2$, and then open with a smaller detectable area change. Note, that at steady state under sufficient tension, a channel with an expandable closed state would go through transitions between the open and closed-expanded states only. Another possible explanation for this discrepancy involves a potential asymmetry of distribution of mechanical force across the liposome membrane. Indeed, due to the absence of integral proteins, the two leaflets of liposome membrane may slide one along another. When tension is applied to the membrane patch the inner leaflet, which is not in contact with the pipette, may relax, and as a result the tension will soon be redistributed to the outer leaflet. Provided that the channel is oriented with its periplasmic side out (for which we have evidence), only the outer part will be subjected to stretch. Tension applied in this manner may be less efficient in driving the transition than a more uniform stretching exerted in the native membrane; therefore, the activation curve may be shallower, and the apparent $\Delta A$ smaller. The question of what part of the protein is more receptive to the stretch force requires special investigation.

## Nonpolar lining of the inner part of the pore and gain-of-function mutations

According to the model, the iris-like expansion of the pore increases the protein surface exposed to water. The random mutagenesis study by Ou and co-workers (1998) revealed a cluster of apolar residues in the N-terminal half of M1 that are very sensitive to polar or charged substitutions. The mutations G22D, G22N, V23A, G26S, or G30R made the channel severely toxic for cells, apparently because it opened at inappropriately low tension (displaying "soft" or gain-of-function phenotype). Further systematic mutagenesis of G22 showed that more hydrophobic substitutions make the channel "stiffer" or more difficult to open (Yoshimura et al., 1999) and led to the conclusion that the change in activating pressure is proportional to the side chain polarity of the substitute relative to that of glycine. In the closed state, L19, G22, and V23 form the hydrophobic constriction in the EcoMscL pore, and are not fully hydrated. We predict that during the "elastic" barrel expansion the apolar lower part of M1 becomes more hydrated. With charged or hydrophilic substitutions in this region, hydration becomes more favorable and water pulled into the channel should increase the equilibrium diameter of the barrel at any given tension, effectively decreasing its resistance to mechanical stress. It should take less tension to reach the critical deformation for opening from such pre-expanded conformation. Conversely, a more hydrophobic interior should make the channel "stiffer" and harder to open. The sensitive cluster is located near the cytoplasmic end of M1; thus expansion of this region should favor opening because the cytoplasmic end of M1 is linked to the putative S1 gate helices. Peculiarly, the G22K and G22N mutants exhibit stabilization of the first subconducting state (Yoshimura et al., 1999). We assume that five charged (K) or bulky hydrophilic (N) side chains crammed into the narrow lower part of the pore will expand the barrel and pre-stress the S1-M1 linkers almost to the critical point. A minute tension would provoke the transition to S1, which increases the area and thereby relieves the short-range internal conflict in the barrel. Note, that the subsequent S1$\rightarrow$O transitions together bring only small area change and require substantial additional tension ($>$100 mM Hg) so clearly demonstrated by Yoshimura. Thus, the pre-expanded state would create a situation in which the local energetic minimum in the absence of tension for G22K or G22N is not the closed, but the S1 state.

## MscL kinetics and S1 conformations

Under conditions of low open probability, wild-type MscL has at least three components in its open time distribution with mean values of $\sim$37, 6, and 0.3 ms (Blount et al., 1996b). Our model suggests that after disruption of the gate bundle, the liberated S1 helices may preferentially interact with tilted M1, M2, and S3 helices of adjacent subunits. Such "docking" of S1 to the inner surface of the barrel is postulated to confer the long

open time component by stabilizing the open conformation. These interactions are predicted to be mostly between apolar residues (see Table 1 for interactions of residues 1–11 of the open conformation with other residues). Virtually every substitution of a hydrophilic residue for G22, with the exception of glutamate, favors substates while drastically shortening openings to the fully open conformation (Ou et al., 1998; Yoshimura et al., 1999). Yoshimura and coworkers interpreted their data to indicate that G22 is exposed only in the intermediate S1 conformation but is buried when the channel opens. This interpretation is consistent with our models; in the expanded-closed conformations G22 is exposed, whereas in the open conformation G22 is covered by hydrophobic residues at the N-terminus of S1 (it lies between Met-1 and Ile-3). Their finding that the G22E mutant does not favor the substate over the open conformation also is consistent with our open conformation models because the negatively charged group of E22 may bind to the positively charged N-terminus amine and interact favorably with the N-terminus dipole of the S1 helix.

### The periplasmic loop

In the open conformation the loop is modeled as a $\beta$ hairpin lining the outer part of the pore. If the loop is made shorter ($\Delta$Q56) the channel opens only at high tension, showing "stiff" phenotype (Blount et al., 1996b). In contrast, proteolytic cleavage of the loop makes the channel "softer" or easier to open (Ajouz et al., 2000). The loop may well be a "spring" element limiting the expansion of the outer part of the barrel. The reduced length of the loop in $\Delta$Q56 may restrain the wide-open conformation, thus it may take more tension to open the channel. Aromatic substitutions for Q56 in the periplasmic loop of the EcoMscL make openings very long, i.e., they stabilize the open state (Blount et al., 1996b). In our model of the open conformation, Q56 is the only hydrophilic residue of the loop that extends away from the channel and contacts the lipid headgroup region. Thus aromatic residues, especially tyrosin or tryptophan, may "anchor" the loop in the lipid (White and Wimley, 1999) and this would favor open conformations of the barrel and prolong the open state.

In conclusion, the presented models provide the structural framework for the hypothetical gating mechanism of MscL, which implies interplay of two gates placed in series. The modeling permitted us to predict the general tendencies of movement of transmembrane domains during barrel expansion. It helped identify the cytoplasmic (S1) gate and major components involved in functioning of the S1 gate, such as expandable barrel and linkers. It also suggests that the hydration of the pore surface may critically contribute to the resting state of the barrel, and thus determine the tension set point for MscL activation. The models are in agreement with the existing phenomenology, but not completely verified. The secondary structures of the S1 and S2 segments, the hypothesis that the M1-M2 interaction between adjacent subunits remains unchanged during gating, and the hypothesis that S2 and S3 form part of the lipid-exposed outer wall when the channel opens, should be tested. Site-directed mutagenesis, cysteine trapping, and possibly use of fluorescent probes in conjunction with patch-clamp measurements may well serve as low-resolution approaches. Cysteine mutagenesis combined with chemical stabilization of the expanded or open channel conformation reported recently (Yoshimura et al., 2001) now opens new possibilities for high-resolution crystallographic studies of the gating mechanism of MscL.

## APPENDIX 1

### Source of MscL Sequences

| Organism | Data Bank Source |
|---|---|
| *Bacillus subtilis* | sp\|P94585 |
| *Bradyrhizobium japonicum* | gb\|AAF04321.1 |
| *Clostridium histolyticum* | dbj\|BAA77454.1 |
| *Clostridium perfringens* | sp\|P53380 |
| *Deinococcus radiodurans* | gb\|AAF11965.1 |
| *Erwinia carotovora* | sp\|O68284 |
| *Escherichia coli* | sp\|P23867 |
| *Haemophilus influenzae* | sp\|P44789 |
| *Mycobacterium leprae* | emb\|CAB36692.1 |
| *Mycobacterium tuberculosis* | sp\|O53898 |
| *Pseudomonas fluorescens* | sp\|O68286 |
| *Staphylococcus aureus* | sp\|O68285 |
| *Synechocystis sp.* | sp\|P73553 |

*Unfinished Genomes*

| Organism | gnl |
|---|---|
| *Actinobacillus actinomycetemcomitans* | OUACGT\|A.actin_Contig587 |
| *Bordetella bronchiseptica* | Sanger_518\|bbronchi_Contig2331 |
| *Bordetella pertussis* | Sanger\|B.pertussis_Contig1102 |
| *Caulobacter crescentus* | TIGR_76\|C.crescentus_gcc_1680 |
| *Chlorobium tepidum* | TIGR\|C.tepidum_354 |
| *Corynebacterium diphtheriae* | Sanger_1717\|cdiph_Contig419 |
| *Enterococcus faecalis* | TIGR\|gef_6314 |
| *Klebsiella pneumoniae* | WUGSC_573\|kpneumo_B_KPN.Contig1123 |
| *Mycobacterium avium* | TIGR\|M.avium_124 |
| *Mycobacterium bovis* | Sanger_1765\|mbovis_Contig787 |
| *Neisseria gonorrhoeae* | OUACGT\|ngon_Contig161 |
| *Pasteurella multocida* | CBCUMN_747\|Pmultocida.990709.Con372 |
| *Porphyromonas gingivalis* | TIGR\|P.gingivalis_18 |
| *Pseudomonas aeruginosa* | PAGP\|Paeruginosa_Contig204 |
| *Salmonella paratyphi* | WUGSC_32027\|spara_B_SPA.0.25124 |
| *Salmonella typhimurium* | WUGSC_99287\|stmlt2-D2.Contig849 |
| *Shewanella putrefaciens* | TIGR\|S.putrefaciens_5527 |
| *Sinorhizobium meliloti* | Stanford_382\|smelil_423067G02.x1 |
| *Streptococcus pneumoniae* | TIGR\|stp_4142 |
| *Streptococcus pyogenes* | OUACGT\|spyogenes_Contig270 |
| *Thiobacillus ferrooxidans* | TIGR_920\|t_ferrooxidans_249 |
| *Vibrio cholerae* | TIGR\|GVCCM23F |
| *Yersinia pestis* | Sanger\|Y.pesits_Contig927 |

## APPENDIX 2

### Ridge-into-groove-packing

Criterion 6, which favors helix interactions predicted by knobs-into-holes (Crick, 1953) or ridges-into-grooves (Chothia et al., 1981), is our least stringent. Due to the large variance in the size and shapes of amino acid side chains, surfaces of most $\alpha$-helices do not display regular periodic patterns that can accurately be described as either knobs and holes or ridges and grooves. Bowie's (1997b) analysis of helix packing in water-soluble proteins of known structure indicates no statistically significant preference for the helical pair crossing angles ($\Omega$), predicted by these theories. In contrast, his similar analysis of membrane proteins (Bowie, 1997a) did find preferences. For example, $\Omega$ values between 0 and 30° (which are consistent with coiled-coil or 3–4 ridges-into-grooves-type packing) were observed 3.6 times more often than $\Omega$ values between 0 and −30°. Due to the preferential orientation of helices along the normal of the membrane, large absolute $\Omega$ values were rarely observed. However, Bowie reported eight interactions with $\Omega$ between −40 and −60° (consistent with 4–4 ridges-into-grooves packing); whereas only four interactions with $\Omega$ between 40 and 60° were found.

The authors thank Dr. Andrey Anishkin for helpful comments and advice. Part of this work was funded by NASA (NAG2-1452) and National Institutes of Health (NS39314) Research Grants (to S.S.).

## REFERENCES

Ajouz, B., C. Berrier, M. Besnard, B. Martinac, and A. Ghazi. 2000. Contributions of the different extramembranous domains of the mechanosensitive ion channel MscL to its response to membrane tension. *J. Biol. Chem.* 275:1015–1022.

Ajouz, B., C. Berrier, A. Garrigues, M. Besnard, and A. Ghazi. 1998. Release of thioredoxin via the mechanosensitive channel MscL during osmotic downshock of *Escherichia coli* cells. *J. Biol. Chem.* 273: 26670–26674.

Andersen, O. S., C. Nielsen, A. M. Maer, A. Lundbaek, M. Goulian, and R. E. Koeppe II. 1999. Ion channels as tools to monitor lipid bilayer-membrane protein interactions: gramicidin channels as molecular force transducers. *Methods Enzymol.* 294:208–224.

Batiza, A. F., I. Rayment, and C. Kung. 1999. Channel gate! Tension, leak and disclosure. *Structure Fold Des.* 7:R99–R103.

Berrier, C., A. Garrigues, G. Richarme, and A. Ghazi. 2000. Elongation factor Tu and DnaK are transferred from the cytoplasm to the periplasm of *Escherichia coli* during osmotic downshock presumably via the mechanosensitive channel mscL. *J. Bacteriol.* 182:248–251.

Blount, P., and P. C. Moe. 1999. Bacterial mechanosensitive channels: integrating physiology, structure and function. *Trends Microbiol.* 7:420–424.

Blount, P., M. J. Schroeder, and C. Kung. 1997. Mutations in a bacterial mechanosensitive channel change the cellular response to osmotic stress. *J. Biol. Chem.* 272:32150–32157.

Blount, P., S. I. Sukharev, P. C. Moe, S. K. Nagle, and C. Kung. 1996a. Towards understanding of the structural and functional properties of MscL, a mechanosensitive channel in bacteria. *Biol. Cell* 87:1–8.

Blount, P., S. I. Sukharev, M. J. Schroeder, S. K. Nagle, and C. Kung. 1996b. Single residue substitutions that change the gating properties of a mechanosensitive channel in *Escherichia coli*. *Proc. Natl. Acad. Sci. U.S.A.* 93:11652–11657.

Bowie, J. U. 1997a. Helix packing in membrane proteins. *J. Mol. Biol.* 272:780–789.

Bowie, J. U. 1997b. Helix packing angle preferences. *Nat. Struct. Biol.* 4:915–917.

Britten, R. J., and F. T. McClure. 1962. The amino acid pool of Escherichia coli. *Bacteriol. Rev.* 26:292–335.

Brooks, B. R., R. E. Bruccoleri, B. D. Olafson, D. J. States, S. Swaminathan, and M. Karplus. 1983. CHARMM: a program for macromolecular energy minimization and dynamics calculations. *J. Comput. Chem.* 4:187–217.

Butler, S. L., and J. J. Falke. 1996. Effects of protein stabilizing agents on thermal backbone motions: a disulfide trapping study. *Biochemistry.* 35:10595–10600.

Chang, G., R. H. Spencer, A. T. Lee, M. T. Barclay, and D. C. Rees. 1998. Structure of the MscL homolog from *Mycobacterium tuberculosis*: a gated mechanosensitive ion channel. *Science.* 282:2220–2226.

Chothia, C., M. Levitt, and D. Richardson. 1981. Helix to helix packing in proteins. *Mol. Biol.* 145:215–250.

Crick, F. H. C. 1953. The packing of $\alpha$-helices: simple coiled-coils. *Acta Crystallogr.* 6:689–697.

Cruickshank, C. C., R. F. Minchin, A. C. Le Dain, and B. Martinac. 1997. Estimation of the pore size of the large-conductance mechanosensitive ion channel of *Escherichia coli*. *Biophys. J.* 73:1925–1931.

Durell, S. R., and H. R. Guy. 1999. Structural models of the KtrB, TrkH, and Trk1,2 symporters based on the structure of the KcsA $K^+$ channel. *Biophys. J.* 77:789–807.

Gullingsrud, J., D. Kosztin, and K. Schulten. 2001. Structural determinants of MscL gating studied by molecular dynamics simulations. *Biophys. J.* 80:2074–2081.

Guy, H. R. 1985. Amino acid side-chain partition energies and distribution of residues in soluble proteins. *Biophys. J.* 47:61–70.

Guy, H. R. 1988. A model relating the sodium channel's structure to its function. *In* Molecular Biology of Ion Channels: Current Topics in Membrane Transport, Vol. 33. W. S. Agnew, T. Claudio, and F.J. Sigworth, editors. Academic Press, San Diego. 289–308.

Guy, H. R., and S. R. Durell. 1994. Using homology in modeling the structure of voltage-gated ion channels. *In* Molecular Evolution of Physiological Processes. D. Fambrough, editor. The Rockefeller University Press, New York. 197–212.

Guy, H. R., and S. R. Durell. 1996. Developing three-dimensional models of ion channels. *In* Ion Channels, Vol. 4. T. Narahashi, editor. Plenum Press, New York. 1–40.

Häse, C. C., A. C. Le Dain, and B. Martinac. 1997. Molecular dissection of the large mechanosensitive ion channel (MscL) of *E. coli*: mutants with altered channel gating and pressure sensitivity. *J. Membr. Biol.* 157:17–25.

Hille, B. 1992. Ionic channels of Excitable Membranes. Sinauer Associates Inc., Sunderland, MA. 295–296.

Komiya, H., T. O. Yeates, D. C. Rees, J. P. Allen, and G. Feher. 1988. Structure of the reaction center from *Rhodobacter sphaeroides* R-26 and 2.4.1: symmetry relations and sequence comparisons between different species. *Proc. Natl. Acad. Sci. U.S.A.* 85:9012–9016.

Liu, W., J. W. Dietmer, and B. Martinac. 1999. Glycine G14, the amino acid essential for electromechanical coupling in gating of the MscL of *E. coli* by mechanical force. *Biophys. J.* 76:203*a*. (abstract).

Miyazawa, S., and R. L. Jernigan. 1999. Self-consistent estimation of inter-residue protein contact energies based on an equilibrium mixture approximation of residues. *Proteins.* 34:49–68.

Oakley, A. J., B. Martinac, and M. C. Wilce. 1999. Structure and function of the bacterial mechanosensitive channel of large conductance. *Protein Sci.* 8:1915–1921.

Ou, X., P. Blount, R. J. Hoffman, and C. Kung. 1998. One face of a transmembrane helix is crucial in mechanosensitive channel gating. *Proc. Natl. Acad. Sci. U.S.A.* 95:11471–11475.

Ponder, J. W., and F. M. Richards. 1987. Tertiary templates for proteins. Use of packing criteria in the enumeration of allowed sequences for different structural classes. *J. Mol. Biol.* 193:775–791.

Rees, D. C., G. Chang, and R. H. Spencer. 2000. Crystallographic analyses of ion channels: lessons and challenges. *J. Biol. Chem.* 275:713–716.

Sukharev, S. I., M. Betanzos, C.-S. Chiang, and H. R. Guy. 2001. The gating mechanism of the large mechanosensitive channel MscL. *Nature.* 409:720–724.

Sukharev, S. I., P. Blount, B. Martinac, F. R. Blattner, and C. Kung. 1994. A large-conductance mechanosensitive channel in *E. coli* encoded by mscL alone. *Nature.* 368:265–268.

Sukharev, S. I., W. J. Sigurdson, C. Kung, and F. Sachs. 1999. Energetic and spatial parameters for gating of the bacterial large conductance mechanosensitive channel, MscL. *J. Gen. Physiol.* 113:525–540.

Vazquez-Laslop, N., H. Lee, R. Hu, and A. A. Neyfakh. 2001. Molecular sieve mechanism of selective release of cytoplasmic proteins by osmotically shocked *Escherichia coli. J. Bacteriol.* 183:2399–2404.

White, S. H., and W. C. Wimley. 1999. Membrane protein folding and stability: physical principles. *Annu. Rev. Biophys. Biomol. Struct.* 28: 319–365.

Yoshimura, K., A. Batiza, and C. Kung. 2001. Chemically charging the pore constriction opens the mechanosensitive channel MscL. *Biophys. J.* 80: 2198–2206.

Yoshimura, K., A. Batiza, M. Schroeder, P. Blount, and C. Kung. 1999. Hydrophilicity of a single residue within MscL correlates with increased channel mechanosensitivity. *Biophys. J.* 77:1960–1972.